Spatial Distribution of Specific N-cycle Microorganisms in Oxic River Sediments

G.D. Jordan

A thesis submitted for the degree of Master of Science (by Dissertation)

Department of Life Sciences

University of Essex

January 2023

Summary:

Anthropogenic nitrogen (N) inputs cause considerable damage to aquatic ecosystems. Anaerobic ammonia oxidising bacteria (anammox bacteria or AnAOB) have an important role in the removal of fixed N in oxic sediments, despite being obligate anaerobes. AnAOB are also important in wastewater bioreactors. Specifically, in complete autotrophic nitrogen removal over nitrite (CANON) bioreactors, AnAOB interact with other N-cycle groups such as ammonia oxidising bacteria (AOB), archaea (AOA), complete ammonia oxidation (comammox) bacteria and denitrifiers. This thesis aims to investigate the spatial localisation of N-cycle groups in relation to AnAOB in oxic river sediments. Here, imaging techniques such as confocal microscopy and catalysed reporter deposition fluorescent *in situ* hybridisation (CARD-FISH) were utilised. In addition, a novel negative staining technique was developed to analyse sediment grain microtopology. This technique allows accurate 3D measurements of nominally non-fluorescent objects using confocal microscopy - in this case the surface of sediment grains. This thesis found that AnAOB exhibit a chasmoendolithic lifestyle – inhabiting anoxic pores on sediment grain surfaces – a strategy not previously observed in bioreactors. Furthermore, analysis of the spatial interactions of AnAOB with complete ammonia oxidising (comammox) bacteria show 35.2% of AnAOB colonies are found within 1 μm of comammox bacteria colonies, suggesting some form of beneficial relationship. In conclusion, we have a previously unknown oxygen avoidance strategy in AnAOB and have further analysed the relationship of AnAOB with other N-cycle groups in oxic sediments.

Acknowledgements

I would like to thank the many people who helped me with the completion of my thesis. I'd especially like to thank my supervisors Dr Philippe Laissue, Dr Corinne Whitby and Dr Boyd McKew for their invaluable advice over the last 18 months. I would also like to thank Dr David Clark for his work collecting the PRINCe sediment samples and advice on statistical tests, Dr Robert Ferguson for his advice on presentations of this research at conferences, and Dr Jorge Fromlette for his talks with Philippe regarding endolithic microbes.

My thanks go to Farid Benyahia for training me on qPCRs, DNA extractions, and for his expert advice. This research occurred over an unprecedented time of laboratory materials shortages, and I would like to thank Aygun Azadova for sharing reagents and materials that were in short supply. Lastly, I would like to thank my partner Adeline Gewinner for supporting me through the writing of this thesis.

Table of Contents

Table of Figure

Abbreviations

AnAOB – anaerobic ammonia oxidising bacteria

Comammox bacteria – complete ammonia oxidising bacteria

AOB – ammonia oxidising bacteria

AOA – ammonia oxidising archaea

N – fixed nitrogen compounds, e.g: ammonia, nitrate.

CLSM – confocal laser scanning microscope

CW – calcofluor white

AO – acridine orange

Chapter 1 - Introduction

1.1 –The Nitrogen Cycle

Microorganisms are fundamental to the cycling of nitrogen (N), particularly in riverine systems, where they convert ~40% of terrestrial N runoff per year (~47 Tg) to N_2 gas which enters the atmosphere (Galloway *et al.,* 2004). Anthropogenic nitrogen accounts for more than half of the Earth's current fixed nitrogen load, resulting in a decoupling of nitrogen fixation and nitrogen loss and the resultant accumulation of fixed nitrogen in ecosystems. This increased nitrogen load is due to a combination of activities – agriculture, transport, industry etc. (Galloway *et al*., 2003). As of 2009, anthropogenic fixed nitrogen production is four times the safe, sustainable level (Rockström *et al*., 2009). Some fixed nitrogen species can damage both human health and environmental stability. In waterways, increased fixed nitrogen loads can lead to eutrophication. The cost of eutrophication to the UK alone has been estimated at £75-114.3 million per annum, with current policy responses alone costed at £54.8 m (Pretty *et al*., 2003). In the US, costs of eutrophication are calculated to be $2.2 billion annually (Dodds *et al*., 2009).

Eutrophication is linked to the bioavailability of both fixed nitrogen and phosphates; for this reason, the UK Environment Agency currently aims to control concentrations of both (Spears *et al*., 2018). Historically, most focus has been on denitrification as a method to remove fixed nitrogen. However, the spiralling levels of fixed nitrogen in the environment (Galloway *et al*., 2003) suggest that manipulation of denitrification alone is not enough to combat anthropogenic fixed nitrogen release. As such, alternative methods are currently being explored to reduce fixed nitrogen loads. Using AnAOB-based wastewater bioreactors is one such method and has seen success since its

discovery (Kartal *et al*., 2010). Benefits of using AnAOB in bioreactors include reduced oxygen and organic carbon consumption (Ma *et al*., 2020).

Nitrification (i.e., the oxidation of ammonium to nitrate via nitrite) is a key step in the N-cycle (Fig 1.1). Nitrification was previously considered a two-step process, involving two functionally distinct groups of chemolithoautotrophs (ammonia-oxidising archaea (AOA) or ammonia-oxidising bacteria (AOB) that utilise ammonia monooxygenase (encoded by the *amoA* gene) (McTavish *et al*., 1993; Treusch *et al*., 2005), and nitrite oxidising bacteria (NOB), which contain nitrite oxidoreductase (encoded by the *nxr* gene) (Pester *et al*., 2014). However, the discovery of the complete oxidation of ammonia to nitrate (comammox) by a nitrifying bacterium from the genus *Nitrospira* completely changed the paradigm that nitrification requires two distinct functional groups of microbes (Daims *et al*., 2015). Based on *amoA* gene sequences from metagenomes, comammox organisms were shown to belong within Nitrospira lineage II (Daims *et al*., 2015; Koch *et al*., 2019). However, since comammox bacteria do not form a monophyletic group within Nitrospira lineage II, comammox and canonical nitrite-oxidizing *Nitrospira* bacteria cannot be distinguished by 16S rRNA-based methods and the *amoA* gene variant for commamox is used instead as a functional biomarker (Pjevac *et al*., 2017). Since the discovery of comammox, questions have been raised about the role of completely nitrifying *Nitrospira* in N-cycling communities (Daims *et al*., 2015).

Nitrate produced via nitrification can be assimilated into organic N-compounds, be reduced to ammonium via dissimilatory nitrate reduction to ammonium (DRNA), or enter the denitrification pathway (Lehnert *et al*., 2018). Denitrification is the step-wise reduction of nitrate to nitrite, then nitric and nitrous oxide into dinitrogen gas, and represents one of two nitrogen loss pathways, alongside anammox (van de Graaf *et*

al., 1995; Lehnert *et al*., 2018). Denitrification involves three intermediary compounds – nitrite (NO_2^-), nitric oxide (NO) and nitrous oxide (N_2O). The first step is the reduction of nitrate into nitrite, catalysed by nitrate reductases, which can be divided into assimilatory nitrate reductases (Nas, NirA) and dissimilatory nitrate reductases, which are further subdivided into membrane bound (Nar) and periplasmic (Nap) types (Kuypers *et al*., 2018). The second step, the reduction of nitrite into nitric oxide, is catalysed by nitrite reductase enzymes, which can be either cytochrome-based (NirK) or copper-based (NirS) (Braker *et al*., 2000). Finally, nitric oxide is reduced into nitrous oxide, and then into dinitrogen gas, which is catalysed by nitric oxide reductase (Nor) or nitrous oxide reductase (Nos) respectively (Kuypers *et al*., 2018). Nitrate reduction can also be carried out by archaea and eukaryotes (Cabello *et al*., 2004; Fischer *et* al., 2005; Kamp *et al*., 2015). Sequencing studies showing the presence of both assimilatory and dissimilatory nitrate reductase genes in archaeal species across both Crenarchaeota and Euryarchaeota (Cabello *et al*., 2004).

Another pathway for nitrate involves anaerobic ammonia oxidation. Anaerobic ammonia oxidising bacteria (anammox bacteria or AnAOB) were first reported in 1995 as possessing a distinct nitrogen loss pathway (van de Graaf *et al*., 1995). AnAOB convert ammonium and nitrite into dinitrogen using hydrazine as an intermediary compound. The enzymes involved – hydrazine synthase (Hzs) and hydrazine oxidoreductase (Hzo) are unique to AnAOB, and as such the encoding genes (*hzs* and *hzo* respectively) are useful biomarkers (Kartal and Keltjens, 2016). Hzs catalyses the synthesis of hydrazine – an intermediary step in the anammox pathway, while Hzo catalyses the reduction of hydrazine into dinitrogen (Kartal and Keltjens, 2016). AnAOB require both ammonia and nitrite for dinitrogen production, but lack enzymes capable of nitrification, instead relying on nitrite produced by other functional groups

such as ammonia oxidising bacteria (AOB) and archaea (AOA) (Straka *et al*., 2019). Recent evidence suggests that AnAOB can also utilize nitrite produced by complete ammonia oxidising (comammox) bacteria in engineered environments (Gottshall *et al*., 2021).

Coupled nitrification-denitrification, anammox and DRNA interact to regulate reactive nitrogen loads. While denitrification and anammox represent nitrogen loss pathways, DRNA represents fixed nitrogen recycling rather than loss. While DRNA is a nitrogen recycling process, it can still interact with other processes to increase nitrogen loss; anammox and DRNA have been shown to interact in a way beneficial to nitrogen loss in minimum oxygen zones, as DRNA can provide an alternative source of ammonium for AnAOB (Kalvelage *et al*., 2011).

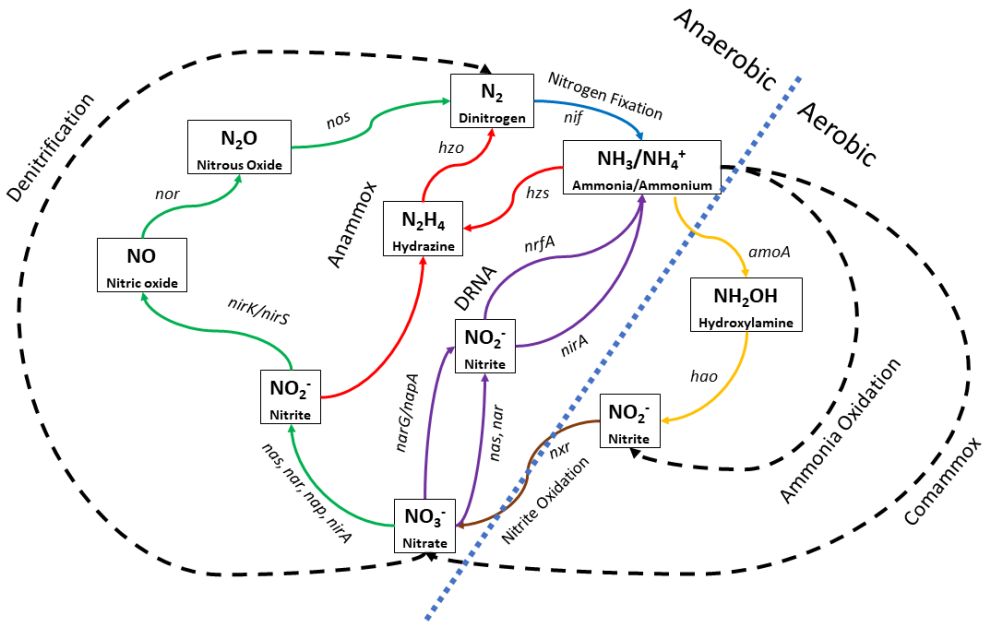

Fig. 1.1 The nitrogen cycle showing intermediary compounds, key genes, anaerobic and aerobic processes. Nitrogen fixation is represented by light blue, ammonia oxidation by yellow, nitrite oxidation by brown, denitrification by green, anammox by red and DRNA by purple. N-assimilation by primary producers has been excluded from this diagram. It should be noted that N-cycle processes are more interactive than is shown. For example, DRNA can use environmental nitrite produced by ammonia oxidation and does not necessarily start with nitrate.

1.2 - Anammox and Community Structure

Anammox is very important for the removal of fixed N and is estimated to be responsible for the removal of 30-70% of fixed N from the environment (Kartal and Keltjens, 2016). Furthermore, AnAOB are responsible for the removal of 58% of fixed N in porous sediments and 7% in non-porous sediments (Lansdown *et al*., 2016). As such, manipulating AnAOB could prove highly beneficial in controlling increasing fixed N loads. Thus, the manipulation of anammox in rivers would subsequently reduce fixed N loads in estuarine and marine environments. Porous sediment types have notably long water residence times (Heppell *et al*., 2017), making management responses slow and challenging, so manipulating AnAOB (important in porous sediments) could greatly aid N management.

Porous river sediments are oxic, yet the results from Lansdown *et al.* (2016) show AnAOB have a more key role in porous than non-porous sediments. Non-porous sediments may both limit the oxygen required for ammonia oxidation while simultaneously limiting diffusion of nitrite into deeper, sub-oxic layers where AnAOB can survive, thus promoting full oxidation of ammonia into nitrate by NOB (Lansdown *et al*., 2016). This hypothesis assumes that the relationship between AnAOB and AOA/AOB is weaker in non-porous sediment than porous (Lansdown *et al*., 2016). The dominance of AnAOB in porous sediments, despite being oxic environments, could be due to two possible factors. The first is the presence of anoxic microsites inside porous, oxic sediments. This would provide a safe niche for AnAOB inside the normally oxic environment. The second is community structure; whereby it is possible that AnAOB exist as part of a community structure with AnAOB in the centre, surrounded by AOA, AOB and NOB. This would provide a ready source of nitrite while simultaneously limiting access to molecular oxygen – molecular oxygen would be used

in oxidation of nitrogen compounds prior to reaching AnAOB, as in CANON bioreactors (Hu *et al*., 2013; Cao *et al*., 2017).

1.3 - Phosphate's Role in AnAOB, AOA, AOB and NOB Relationship

Unlike denitrification, which is regulated by nitrogen and carbon bioavailability, the activity of AnAOB appears to be regulated by the bioavailability of N and phosphate. Lower phosphate levels favour anammox over nitrite oxidation (Nowak *et al*., 1996). Furthermore, lower phosphate levels lead to an overall increase in dinitrogen production (French *et al*., 2012). This is because low phosphate levels significantly lower the rate of nitrite oxidation (Nowak *et al*., 1996) while having a lesser effect on ammonia oxidation (Purchase, 1974) as shown in Fig. 1.2. This is likely responsible for the results observed in French *et al.* (2012) whereby lower phosphate levels reduced the rate at which nitrite is being oxidised into nitrate by NOB, while having a lesser effect on ammonia oxidation. This would result in the accumulation of nitrite and ammonia, resulting in an ideal environment for anammox activity, which in turn would result in increased dinitrogen production (French *et al.*, 2012). This is due to i) anammox results directly in dinitrogen production, whereas nitrate produced by NOB must further undergo denitrification before dinitrogen is produced. Produced nitrate does not necessarily enter denitrification, but may instead be taken up by primary producers, resulting in fixed nitrogen remaining in the environment; ii) anammox results in the loss of nitrogen from both nitrite and ammonia, meaning twice as much nitrogen is removed from the environment in each reaction. These two factors make anammox a more efficient pathway for nitrogen loss (Kartal and Keltjens, 2016). It is currently unknown if the changes caused by phosphate levels are due to changes in gene regulation or changes in the population numbers of the organisms involved.

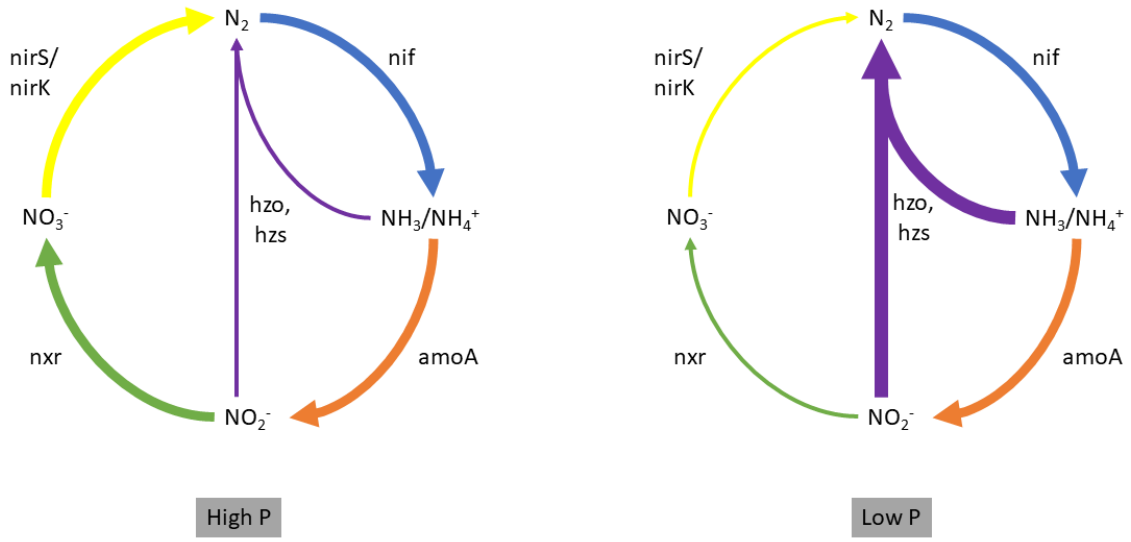

Fig. 1.2: Regulatory role of phosphorus in key microbial N-cycle processes. Key functional genes/biomarkers are highlighted for each process. Nitrogen fixation is represented by blue, ammonia oxidation by orange, nitrification by green, denitrification by yellow and anammox by purple. Comammox has been excluded from this diagram.

The UK Environment Agency already aims to control phosphate levels due to the influence of phosphate eutrophication and subsequent algae growth (Spears *et al*., 2018). The regulatory effect of phosphates on the anammox-nitrification relationship gives more emphasis on controlling P levels. P, alongside N, is the primary driver of eutrophication (Correll, 1998). The impact of P levels on comammox bacteria is yet unknown. However, some bioreactor-based studies on the relationship between partial nitrification, comammox and anammox processes exist (Wu *et al*., 2019). For example, Wu *et al*. (2019) found that the three processes can co-operate in differing niches to achieve a 98.82% removal efficiency for ammonium. It is possible that the relationship between comammox and anammox is impacted by phosphate levels. While future studies may prove this, it is not in the remit of this thesis to examine this.

1.4 - Diversity and Distribution of AnAOB, AOA, AOB, Comammox Bacteria, NOB, and Denitrifying Bactria

AnAOB consist of several genera in the phylum Planctomycetota and are characterised by possessing an anammoxosome – an internal compartment with a single ladderlane lipid membrane (van Niftrik *et al*., 2004). Environmental genomics studies of the *hzo* gene show that AnAOB are widely distributed across many environments, although the diversity of AnAOB varied widely across differing environments (Hirsch *et al.,* 2011). Hirsch *et al.* (2011) found that deepwater samples have the highest observed species richness when analysed using *hzo* environmental genomics, followed by riverine sediment, groundwater and estuarine sediment (Hirsch *et al*., 2011). However, it is to be noted that riverine and estuarine sediment samples in this study were collected from one particular river – the Cape Fear River – and may not accurately reflect AnAOB diversity across different river geologies, particularly in light of the differing dominance of AnAOB across sediment types as shown by Lansdown *et al.* (2016).

While AnAOB diversity can be assessed using 16S rRNA gene primers, this approach has been shown to be flawed. The highly conserved nature of 16S rRNA cannot account for the diversity found in AnAOB. Research (Hirsch *et al*., 2011) shows *hzo* – a gene unique to AnAOB – to be a better indicator of the diversity present. For example, Hirsch *et al.* (2011). found a species richness of 17 in riverine sediment when assessed by *hzo* primers, but only 8 when assessed by 16S rRNA gene primers.

Ammonium oxidation occurs in a phylogenetically diverse set of microorganisms stretched across two domains; ammonia-oxidising archaea (AOA) and bacteria (AOB). The evolutionary relationship between both groups remains ambiguous – archaeal

AmoA and bacterial AmoA differ significantly in structure, and possibly function (Simon and Klotz, 2013). AOA belong to the phylum Thaumarchaeota and more specifically to the class *Nitrososphaeria* (Alves *et al*., 2018). Marine and Freshwater AOA show evidence of niche differentiation based on depth, and terrestrial AOA by pH level (Alves *et al*., 2018). There is also evidence of niche differentiation between AOA and AOB based on acidity and ammonium concentration, whereby, in general, AOA are dominant in acidic and low ammonium soils. Dominance of AOA in low ammonium soils is due to a generally higher ammonium affinity (Prosser and Nicol, 2012; Clark *et al.*, 2020; Jung *et al*., 2021; Scarlett *et al.*, 2021). An exception to this is the genus *Nitrosocosmicus* (Jung *et al*., 2021).

AOB consist of three known genera – *Nitrosomonas*, *Nitrosococcus* and *Nitrosospira*, of which *Nitrosomonas* and *Nitrosospira* are members of the Betaproteobacteria. *Nitrosococcus* is a member of the Gammaproteobacteria (Head *et al*., 1993) *Nitrosococcus*, with few exceptions, is a marine genus, whereas *Nitrosomonas* and *Nitrosospira* are freshwater and soil AOB (Hovanec and DeLong, 1996; Ward and O'Mullan, 2002). *Nitrosomonas* and *Nitrosospira* have demonstrated niche differentiation (Ke *et al*., 2013). *Nitrosomonas* species are dominant in areas with high ammonium concentrations, such as wastewater bioreactors. *Nitrosospira* are dominant in areas with lower ammonium concentrations, such as soils (Lehtovirta-Morley, 2018). Comammox bacteria represent a polyphyletic group within *Nitrospira* lineage II (Daims *et al*., 2015; Koch *et al*., 2019). Comammox bacteria are distinguished by a unique *amoA* gene mutant allowing complete oxidation of ammonia (Pjevac *et al*., 2017).

Nitrite oxidising bacteria (NOB) are divided into six genera; *Nitrobacter, Nitrospira, Nitrotoga, Nitrococcus, Nitrospina* and *Nitrolancetus* (Gould and Lees, 1960; Watson

and Waterbury, 1971; Daims *et al*., 2001; Alawi *et al*., 2007; Sorokin *et al*., 2012). Of these, *Nitrospira* and *Nitrobacter* are important in terrestrial ecosystems (Bartosch *et al*., 2002; Ke *et al*., 2013). Terrestrial NOB genera show niche differentiation based on metabolic attributes. *Nitrobacter*-like NOB prefer high substrate concentrations while having lower substrate affinity, whereas *Nitrospira*-like NOB prefer lower substrate concentrations while having higher substrate affinity. *Nitrobacter*-like NOB have higher growth rates to take advantage of higher substrate concentrations (Daims *et al*., 2001; Blackburne *et al*., 2006; Nowka *et al*., 2015).

Denitrifying bacteria are a very diverse group. Riverine denitrifying bacteria contain species across the Bacteroidetes, Alphaproteobacteria, Betaproteobacteria, Gammaproteobacteria, Epsilonproteobacteria Actinobacteria, Cyanobacteria, and Firmicutes classes (Zhang *et al*., 2021). Members of the *Thiobacillus*, *Halomonas*, *Pseudomonas*, *Flavobacterium*, *Bacillus*, *Arthrobacter*, *Hyphomicrobium*, *Rhodobater*, *Hydrogenophaga*, and *Denitrastisoma* genera are the most common (Zhang *et al*., 2021). There is some debate regarding the reason for this diversity (Braker and Conrad, 2011). It is generally assumed that high diversity results in effective communities due to occupying more niches, something supported by some studies into denitrifier diversity (Salles *et al*., 2009). However, other experimental evidence shows that denitrification is unaffected by diversity (Wertz *et al*., 2006; Wertz *et al*., 2007).

1.5 – Lithobiont Classifications

One of the hypotheses forwarded in this thesis suggests a lithobiotic lifestyle for AnAOB. Lithobionts are organisms that colonise rocky substrates. Lithobionts can be divided into two groups based on their method of colonising grains: epiliths and

endoliths. The locations of different lithobiotic groups can be seen in Fig. 1.3. Epiliths colonise the surface of sediment grains, inhabiting regions of the surface that are sheltered by microtopography (Probandt *et al*., 2018). Endoliths, in comparison, inhabit the sediment grain itself. Endoliths can be further subdivided into chasmoendoliths and cryptoendoliths. Chasmoendoliths inhabit chasms and fissures on the grain surface, whereas cyptoendoliths colonise pores and cavities within grains. Some endoliths merely take advantage of already-present features, whereas others – euendoliths - are capable of biogenic engineering – penetrating the surface of grains to create new chasms or pores (Wierzchos *et al*., 2011). Some organisms use both epilithic and endolithic strategies, such as lichen (Castro-Sowinski, 2019). Only three groups are known for euendolithic boring activity: euendolithic cyanobacteria, fungi and algae (Ramírez-Reinat and Garcia-Pichel, 2012). A common form of boring in calcium-based rocks (such as chalk) involves using acid produced as a metabolic biproduct. This is a mechanism present in some heterotrophic aerobic bacteria, fermenting sulphide-oxidising, and nitrifying bacteria (Garcia-Pichel, 2006). The production of acids has also been suggested as a mechanism for boring in fungi, algae, and cyanobacteria (Garcia-Pichel, 2006). Some boring organisms form biofilms (de los Ríos *et al*., 2006). As AnAOB do not belong to any of these clades, a discovery of endolithic AnAOB would suggest two possibilities: that AnAOB are a fourth, unknown group capable of euendolithic boring, or that AnAOB possess a symbiotic/commensalist relationship with one or more of the above groups.

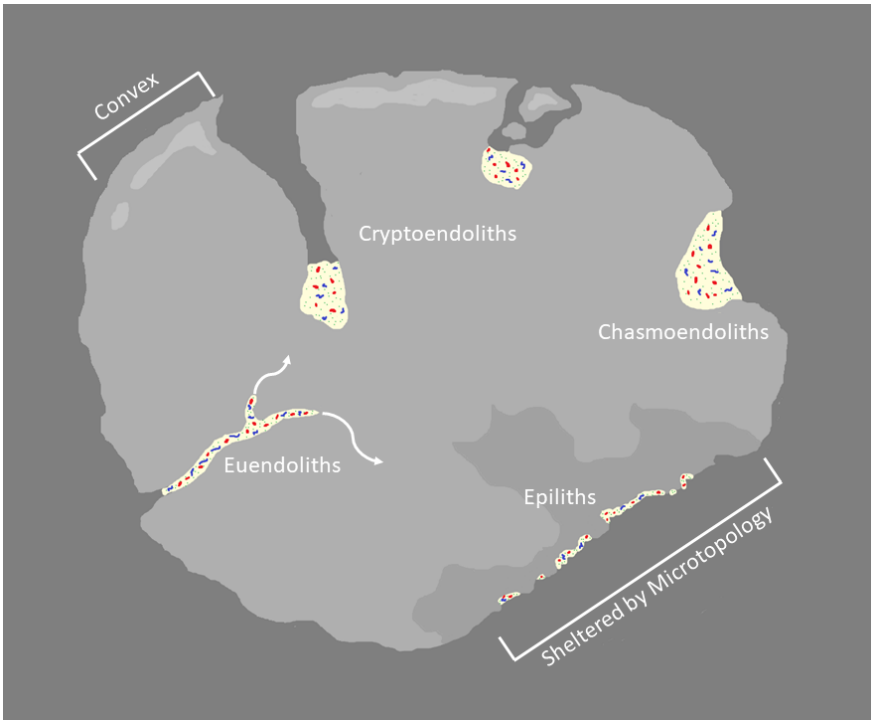

Fig. 1.3: Colonisation strategies and classifications of lithic microorganisms. Rock is shown in light grey, biofilms in beige. The microtopological difference between convex and sheltered areas is demonstrated and labelled. Diagram shows endolithic, cryptoendolithic, chasmoendolithic and epilithic microorganisms. Epilithic niches consist of sheltered surface areas, chasmoendolithic niches consist of chasms burrowed into the surface, cryptoendolithic niches consist of deep pores and cavities inside the grain. Eundolithic organisms are capable of biogenic engineering to produce new niches.

1.6 - Fluorescent *in-situ* Hybridisation Microscopy

FISH (fluorescent *in situ* hybridisation) involves the tagging of genetic material via hybridising probes. The specificity of this process allows the tagging of particular genes or regions of DNA (Speicher and Carter, 2005). FISH can also be used on mRNA or other extra-chromosomal genetic material (Raj *et al*., 2008). FISH involves the hybridisation of a complementary probe to the target sequence (Ratan *et al*., 2017). There are several methods for producing the complementary probe described in Speicher and Carter (2005) – nick transformation, random-primed labelling and PCR - Fig. 1.4 shows the different methods of labelling probes. Probe labelling can be either direct or indirect – complementary probes can be made with modified fluorescent

nucleotides or be given binding sites (called haptens) respectively. If probes are labelled indirectly, a secondary step must be undertaken – fluorophores must be immunologically or enzymatically bound to haptens for fluorescence to occur (Speicher and Carter, 2005). While direct labelling is simpler, indirect labelling allows signal amplification, and as such as superior fidelity (Speicher and Carter, 2005). Hybridised probes can be viewed through several different fluorescence microscope types, including widefield or laser scanning confocal (LSCM) microscopes, with LSCMs giving superior resolution to widefield (Wada *et al*., 2016).

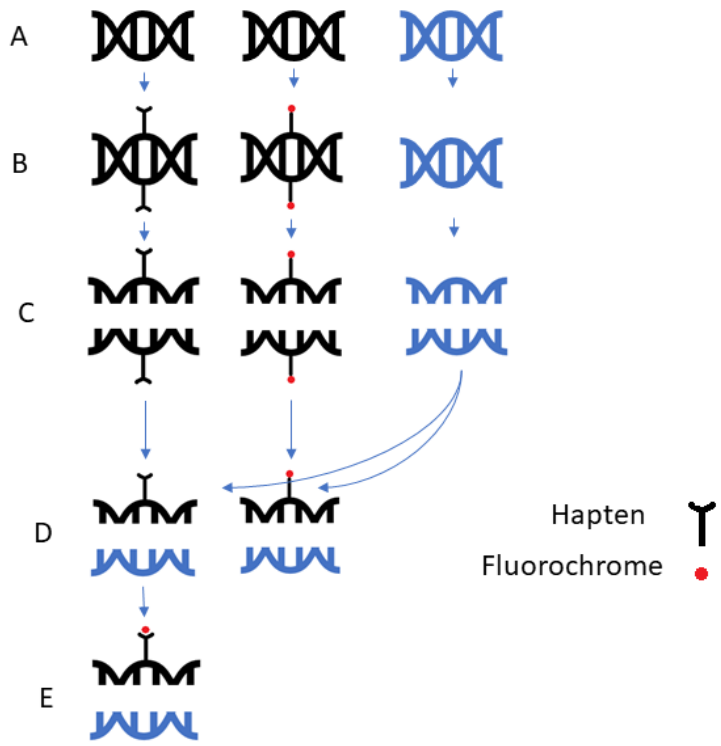

Fig. 1.4: Difference in probe formation and use in FISH bioimaging for DNA. The left column demonstrates the use of an indirect probe using a hapten. The middle column demonstrates the use of a direct probe. Stage A represents the initial starting genetic material. Stage B represents the attachment of either haptens (indirect) or fluorochromes (direct). Stage C is the denaturing of genetic material. Stage D represents the hybridisation of probes and the target genetic material. Stage E represents the immunological addition of fluorochromes to haptens.

There are several problems associated with fluorescence microscopy, such as aspecific binding and background autofluorescence (Wada *et al*., 2016). Many troubleshooting methods have been created to deal with problems in FISH, listed in the review paper Wada *et al.* (2016). One is optical sectioning, which allows the removal of non-specific background autofluorescence. This is possible when using LCSMs. Another option is to use a negative nonsense probe to identify non-specific probe binding. As a nonsense probe is not complementary to any sequence within the genome, it will highlight if non-specific binding is occurring, allowing identification of the problem. Aspecific binding can be detected using complementary negative probes, where binding is blocked by the previously attached probe. An example of this is NON338 (Wallner *et al*., 1993). The use of CARD-FISH – a signal amplification technique – is another troubleshooting option for difficult samples (Wada *et al*., 2016).

1.7 - CARD-FISH Advantages, Disadvantages and Mitigation

CARD-FISH is a superior method to FISH when dealing with low population samples or when targeting functional genes (Wada *et al*., 2016). The principles of CARD-FISH are described in Kubota (2013) and shown in Fig 1.5. CARD-FISH allows the deposition of multiple fluorescent molecules at the same hybridisation site, resulting in greater fluorescence. This allows easier determination of binding sites from background autofluorescence. CARD-FISH works by the principle of tyramide signal amplification, a process requiring horse radish peroxidase (HRP) and haptenized tyramines. Proximity to HRP catalyses the dimerization of tyramines, a process involving highly reactionary intermediaries. When dimerised tyramines leave the proximity of HRP, the reaction will reverse. By using lower concentrations, some reactionary intermediaries will instead bind non-specifically with aromatic compounds. IF HRP is attached to a FISH probe, this causes the deposition of tyramines around

the probe site (Kubota, 2013). If tyramines are fluorescently labelled, this allows greater levels of fluorescence than the single fluorophore labelling seen in the standard FISH methodology (Pernthaler *et al*., 2002).

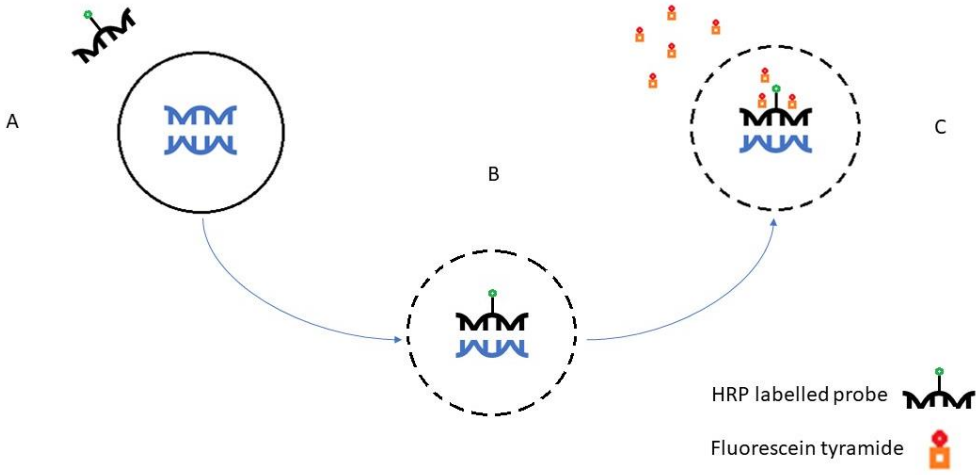

Fig. 1.5: Mechanism of CARD-FISH. Blue represents target DNA, while black represents the complementary gene probe, labelled with HRP. First (A) DNA must be denatured. Then (B) cellular membranes must be permeabilized to allow passage of HRP and the unlabelled probe. Lastly (C), a wash of fluorescently labelled tyramides is applied. HRP catalyses the creation of reactive tyramide intermediaries in proximity, leading to the covalent binding of fluorescently labelled tyramides around tyrosine residues.

While CARD-FISH has advantages over other FISH methods, it also has some disadvantages. CARD-FISH relies on HRP which is a much larger molecule compared to the fluorochromes used in FISH – HRP has a molecular mass of around 40 kDa (Rennke and Venkatachalam, 1979) compared to 300-1000 Da for many fluorochromes (ex. 4′,6-Diamidino-2-phenylindole dihydrochloride (DAPI) has a molecular mass of 350.4 Da (pubchem.ncbi)). The larger size of HRP means an enzymatic permeabilization step must be undertaken for most organisms, although there are exceptions. Responses to various permeabilization techniques vary between phyla (Kubota, 2013). Some microbial groupings such as the phylum Planctomycetota require only fixation, whereas other groups require permeabilization (Kubota, 2013).

This, unfortunately, makes CARD-FISH a difficult technique to use on heterogenous samples (Pernthaler *et al*., 2002).

CARD-FISH is the ideal method for analysing N-cycle microbes that occur in relatively low abundance such as AnAOB (Sonthiphand *et al*., 2014). When analysing freshwater microorganism communities, chloroplast containing organisms can autofluoresce at 488 or 561 nm (Probandt *et al*., 2018). Thus, the combination of low population densities and potentially strong background autofluorescence, suggests that CARD-FISH is ideal for studies of this type, despite the heterogenicity of the sample used.

Several strategies have been developed to improve CARD-FISH signalling. One of the most common techniques is amending the CARD-FISH solution (Kubota, 2013). van Gijlswijk *et al*. (1996) investigated the sensitivity and localisation outcomes for various additive substances and concluded that dextran sulphate and polyvinyl alcohol (PVA) were the best additives. Dextran sulphate addition caused an increase in signal localisation above 10%. However, a decrease in sensitivity occurred above 30% (van Gijlswijk *et al*., 1996). PVA was found to offer the best signal localisation at the expensive of sensitivity (van Gijlswijk *et al*., 1996). It was also noted that dextran sulphate can produce a spotted background unless the post-tyramide wash is performed between 45-60 ˚C. Choice of PVA versus dextran sulphate may depend on whether low sensitivity or poor signal localisation is the primary problem faced.

The addition of inorganic salts or certain organic compounds can also enhance signal strength. Examples of inorganic salts include NaCl and KCl from a concentration of 2 M and higher (Ishii *et al*., 2004). For fluorescent reagents, *p*-iodiophenyl boronic acid is the preferred enhancer (Kubota, 2013). Ishii *et al.* (2004) describes CARD-FISH

imaging of archaea in marine sediment with the application of 2 M NaCl and *p*-iodophenyl boronic acid at 20x the concentration of tyramide as effective. While this is in marine rather than riverine sediment, the environmental similarities mean the same approach may be useful when addressing questions regarding riverine sediments.

1.8 – Image Noise and Processing

Blurring must be removed for image clarity. The point spread function (PSF) describes image burring. The point spread function describes the diffraction of light from an 'infinitely' small point source of light within the specimen and in the case of FISH, this is the fluorochromes contained in the sample. The PSF can be best described as the 3D diffraction pattern from this 1D light source (Born and Wolf, 1980). The PSF can be determined either mathematically using various formulae or measured using a sub-resolution fluorescent point either embedded in the sample or imaged using identical conditions to the sample. This fluorescent point can be used to calculate the PSF using the following equation: image = object (X) PSF, with (X) representing convolution. Once the PSF is calculated, two algorithm types can be used to reduce PSF-derived blurring – deblurring and restoration algorithms – with both having advantages and disadvantages (Swedlow, 2013).

Deblurring algorithms use the surrounding neighbourhood around an illuminated point to deconvolve an image. The sum of illumination at the central point is compared to the sum of illumination in the surrounding area in order to deconvolve the point in question. Deblurring algorithms will process an image one point at a time until the image is completely deconvolved. This method is problematic precisely because it is point by point – PSF of the whole image is not taken into account, leading to erroneous results. As a result, this method is not ideal for point quantification, where restoration

algorithms should be used instead. However, deblurring algorithms do have advantages – they are fast and require little preparation – the PSF does not have to be calculated using the above two methods. As such, they can be used for preliminary examination of images quite effectively (Swedlow, 2013).

Restoration algorithms normally use the PSF calculated by the aforementioned equation to deconvolve an image. Restoration algorithms use an iterative process to improve deconvolving. Blind deconvolution is an extension of restoration algorithms that do not require the calculated PSF, instead guessing PSF based on a number of factors – aperture size, wavelength etc. Restoration algorithms are more accurate than deblurring algorithms but require more effort and computing power (Swedlow, 2013).

Swedlow (2013) concentrates particularly in image processing for quantitative imaging – the type planned for this study, and as a result, the paper is particularly relevant for my topic. Swedlow (2013) also mentions other image clarity issues and associated image processing, such as scattering and rapid variations in laser luminosity due to technical faults. As scattering is stochastic, it is impossible to account for algorithmically in the same way as convolution. Scattering is caused by a poor and variable refractive index (RI) in the sample due to the presence of structures, biological or otherwise (Pawley, 2000; Swedlow, 2013). Laser performance can also impact image noise (Zucker and Price, 2001). Lastly, dark noise – caused by thermal electrons at the detector plate – is also an issue (Bankhead, 2014).

Optical noise can be removed through several methods, with several programs and packages specialised in its removal, such as ImageJ (Schindelin *et al*., 2012) and FISHalyseR (Arunakirinathan and Heindl, 2022). Generally, optical noise can be defined with either a Poisson or Gaussian distribution, with ‘photon noise’ – from the

emission of light itself – following a Poisson distribution. ‘Read noise’ – from detection and reading issues – follows a Gaussian distribution. Photon noise, following a Poisson distribution, is inverse to the number of photons detected, making it particularly problematic in low light samples (e.g: environmental samples with a low quantity of attached fluorophores). ImageJ plugins such as ‘Accurate Gaussian Blur’ can be used to remove noise (Schmid, 2008).

Although there are exceptions, these definitions are the basis for noise reduction in programs such as ImageJ. Functions exist for ‘cleaning-up’ noise caused by Gaussian blurring. As mentioned, dark noise follows neither distribution (Bankhead, 2014).

1.9 – Aims and Rationale

Lansdown *et al.* (2016) showed that AnAOB play an important role in oxic riverine sediments, despite being obligate anaerobes. Two possible explanations for these findings are:

1. Anammox organisms survive in anoxic microsites within otherwise oxic sediments where oxygen concentrations are low enough for their survival, yet ammonium and nitrite can still diffuse into.
2. There exists a co-operative and complex community structure involving N-cycle microorganisms whereby AnAOB live in the centre of a community structure, surrounded by AOB or comammox bacteria, in a similar system to that found in bioreactors. In this scenario, aerobic microorganisms will consume oxygen prior to diffusion into the central anammox community, resulting in a low concentration of oxygen while still allowing AnAOB access to nitrogen compounds.

In order to better understand the role of AnAOB in oxic sediments and address these questions, this thesis aims to develop and optimise protocols (e.g. the use of CARD-FISH) to examine the community structure of N-cycle groups in riverine sediments.

This leads to the following specific **objectives** and **hypotheses**:

Specific Objectives:

Objective 1: Use CARD-FISH to examine the community structure of N-cycle groups within porous riverine sediment (i.e: sand and chalk).

Hypotheses:

Hypothesis 1: AnAOB exist in anoxic microenvironments within porous riverine sediment.

Hypothesis 2: AnAOB inhabit anoxic cores in microbial communities consisting of annamox bacteria, AOA, AOB and NOB, or some combination of these groups.

Hypothesis 3: AnAOB survive in oxic sediments through a combination of the two above mechanisms.

Chapter 2: AnAOB on Sediment Grains

2.1 Introduction

2.1.1 The Importance of AnAOB in the Nitrogen-Cycle

Anthropogenic activity accounts for more than half of the Earth's current fixed nitrogen load, with N levels being four-fold above the sustainable level (Galloway *et al*., 2003; Rockström *et al*., 2009). Despite being anaerobic, AnAOB play a substantial role in N loss in oxic, porous sediments such as chalk and sand (Lansdown *et al*., 2016). In this study, two hypotheses were initially put forward to explain this phenomenon, both based around anoxic microsites. The first hypothesis was based around observations seen in CANON wastewater bioreactors, where the anoxic cores of bacterial flocs are inhabited by AnAOB (Hu *et al*., 2013; Cao *et al*., 2017). The second hypothesis was based on anoxic microsites created by sediment grain microtopology.

2.1.2 Technical Limits to Microscopic Analysis

Examining AnAOB interactions with sediment grain microtopology presents several problems. While FISH-based techniques to examine microbial colonisation of sediment grains have existed for several years, notably being used by Probandt *et al.* (2018) to examine the microbial community on coastal sand grains, this only allows mapping of cell identities and locations without reference to the grain microtopology in 3D, making it impossible to determine cell depths in relation to the grain surface. The inability to determine depth makes it difficult to identify anoxic microsites or to determine if a microbial group is epilithic or endolithic.

Using confocal fluorescence microscopy, only fluorescent objects can be viewed in three dimensions. Non-fluorescent objects can only be viewed with a two-dimensional transmission detection. As fluorescent probes cannot be attached to inorganic surfaces like chalk, sand etc, this means the grain microtopology cannot be viewed in 3D, making it difficult to determine the impact of microtopology on microbial colonisation. Scanning electron microscopy (SEM) can be used to examine colonisation of sediment grains (Beeftink and Staugaard, 1986), but doesn't produce images in true 3D (i.e: depth cannot be accurately measured) and furthermore cannot utilize fluorophore-based techniques (i.e: FISH) to identify microbial groups and processes. For example, SEM would not be able to distinguish AnAOB from other small cocci cells. In order to examine the possibility of anoxic microtopology-based microsites, we have overcome this by developing a method to combine 3D microtopological imaging with fluorescent in-situ hybridisation (FISH) using confocal microscopy.

2.2 – Materials and Methods

2.2.1 – River sites and sediment sampling

Oxic riverine sediment (greensand and chalk) samples were collected from rivers in the Southeast of England (see Fig. 2.1). The rivers Ebble (51.0275, -1.9217), Cray (51.4242, 0.12649), Lambourn (51.4288, -1.3769), Rib (51.8392, -0.0294), Marden (51.3183, -1.86) and Medway (51.268, 0.51844) were sampled. Surficial sediments (0-5 cm) were removed with Perspex cores. Samples consisted of non-vegetated sediment with a heterogenous mixture of coarse (4.75 mm to 9 mm) and non-coarse sediment grains. Proportions of coarse and non-coarse grains varied. Multiple cores were taken from different sites on the same rivers. Sediment was then decanted for use in other experiments (e.g: qPCR). Remaining sediment was then frozen at – 20 °C for long term storage. Unless stated otherwise, samples from sites containing the highest abundance (via qPCR) of *hzo* (hydrazine oxidoreductase coding gene from AnAOB) were used: Ebble (chalk; C1), Cray (chalk; C2), Lambourn (chalk; C3), Rib (chalk; C4) Marden (greensand; S1), Medway (greensand; S2) and Marden (greensand; S3) with *hzo* abundance of 3.5×10^6 g^{-1}, 2.7×10^6 g^{-1}, 2.6×10^5 g^{-1}, 2.9×10^6 g^{-1}, 1.7×10^6 g^{-1}, 1.4×10^6 g^{-1}, 1×10^6 g^{-1} and 9.2×10^5 g^{-1} respectively. Samples were transported in sealed vials then frozen. No additional steps were taken to prevent contamination or manage oxic/anoxic environments.

Table 2.1: Summary of sampling locations discussed in section 2.2.1 – River sites and sediment sampling. Shows sample coding, river name, longitude, and latitude of sampling locations. S1 and S3 are both taken from the same approximate location on the river Marden.

Sample Code	River	Latitude	Longitude
C1	Ebble	51.0275	-1.9217
C2	Cray	51.4242	0.12649
C3	Lambourn	51.4288	-1.3769
C4	Rib	51.8392	-0.0294
S1	Marden #1	51.3183	-1.86
S2	Medway	51.268	0.518
S3	Marden #2	51.3183	-1.86

Fig. 2.1: Co-ordinates of the six sampling sites used in this study. Produced using Google™ Maps.

2.2.2 – Sample Fixation

Crystalline paraformaldehyde (Sigma-Aldrich®) was used to produce a fixative solution of 4% (v/v) formaldehyde in 1x PBS. Paraformaldehyde was heated at 60 °C until dissolved. NaOH was used to adjust fixative solution to pH 7.2. 1x PBS was produced using PBS tablets (Thermo Scientific™ Oxoid™) dissolved in molecular quality water (Water filtered via reverse osmosis; hereby referred to as molecular quality H_2O). For FISH, catalysed reporter deposition-FISH (CARD-FISH) and DAPI (4′,6-diamidino-2-phenylindole) staining, 0.1 g (wet weight) of sediment was fixed in 0.25 mL of 1x PBS and 0.75 mL of the previously described fixative solution. Samples were then inverted three times to mix and incubated overnight at 4 °C. The following day, samples were washed three times with 1x PBS and stored at -20 °C until further use.

2.2.3 - DAPI Staining

DAPI (Invitrogen™) staining was conducted as follows: 120 µL of a 3.3 ng/µL DAPI (in molecular quality H_2O) was used with fixed samples (0.1g wet weight) in 2 mL reaction tubes for 1 h at room temperature in the dark. Tubes were inverted three times to mix. Samples were then washed three times with 1x PBS.

2.2.4 - Acridine Orange and Calcofluor White Staining

Non-fixed sediment[1] (0.1g wet weight) was suspended in 76 µL of 2 µg/µL acridine orange (Invitrogen™) and incubated for 30-min at room temperature in the dark. Sediment was then washed three times with 1x PBS. Following this, the sediment was resuspended in 36 µL of 25 mM calcofluor white (Sigma-Aldrich®) and 36 µL of 10% (v/v) KOH for 3 min. During staining, samples were inverted each minute to mix.

Following staining, samples were washed three times with 1x PBS. Acridine orange was chosen over DAPI due to the overlap in emission spectrums between DAPI and calcofluor white.

1) Fixation isn't necessary for acridine orange and calcofluor white to function, so this step was skipped.

2.2.5 – Direct FISH Staining (Eub338f, AAO258f, NON338 and Amx368f)

Table 2.2: Direct FISH probes used during this study showing probe, associated gene targets, wavelengths of attached fluorophore, the fluorophore type, and the optimal hybridisation buffer for probe binding at 37 °C.

Probe	**Target**	**Absorption (nm)**	**Fluorophore type**	**Hybridisation Buffer Used**
AAO 258f	AOB 16S rRNA (general)	488	Alexa Fluor™	20%
Eub338f	Eubacterial 16S rRNA	488	Alexa Fluor™	40%
NON338	Eubacterial 16S rRNA	565	ATTO	40%
Amx368F	Anammox bacteria 16S rRNA	565	ATTO	30%

Direct FISH labelling was conducted using the following FISH probes; Eubacterial 16S rRNA probe Eub338f (5′-GCTGCCTCCCGTAGGAGT$_{Alexa488}$-3′; Amann *et al*., 1990; Sigma-Aldrich®), Eubacterial 16S rRNA probe NON338 (5′-ACTCCTACGGGAGGCAGC$_{ATTO565}$-3′; Wallner *et al*., 1993; Sigma-Aldrich®), non-marine AOB 16S rRNA probe AAO258f (5′-GCCTTGGTAAGCCTTTACC $_{Alexa488}$-3′; Hastings *et al*., 1997; Sigma-Aldrich®), reversed Eubacterial 16S rRNA control probe NON338 (5′-ACTCCTACGGGAGGCAGC-3′$_{ATTO565}$; Wallner *et al*., 1993; ordered from

Sigma-Aldrich®) and AnAOB 16S rRNA probe Amx368f (5′-CCTTTCGGGCATTGCGAA $_{ATTO565}$-3′; Schmid *et al*., 2003; Sigma-Aldrich®). All direct FISH labelling was conducted on 0.1 g (wet weight) of fixed sediment. Sediment was suspended in 76 µL of 20-40% hybridisation buffer (0.2-0.4 mL formamide, 0.1 mL of 300 mM Tris-HCl (pH 7.2), 10 µL of 10% (w/v) SDS and 0.3-0.5 mL of molecular quality H_2O) and 8 µL of a 50 ng/µL fluorescent probe solution (final concentration in hybridisation buffer of 4.76 ng/µL). Apart from molecular quality H_2O, all components in solution sourced from Sigma-Aldrich®. Hybridisation buffer concentrations for each probe can be found in Table 2.1. Samples were inverted three times to mix. Sediment was then incubated overnight at 37 °C. Sediment was then washed three times with 1x PBS. The following experiments were conducted using this method. AAO258f and Amx368f with N = 3 for both greensand and chalk, and Eub338f with N = 3 for both greensand and chalk. All experiments were counterstained with DAPI.

2.2.6 - Eub338f Controls

Throughout, Eub338f positive controls were conducted using pure cultures of *Escherichia coli* (XL1 blue; Agilent Technologies, Inc). *E. coli* were stored as aliquots at – 80 °C then thawed -20 °C for 30 minutes, then thawed at room temperature (RT) for a further 30 minutes. *E. coli* were then grown at RT in LB broth for 48 h before harvesting. *E. coli* cells were fixed as previously described, then hybridised with Eub338f in 40%, 30% or 20% (v/v) formamide solutions to determine the optimal hybridisation buffer. Optimal hybridisation buffer was also determined for the other probes listed above, including negative control NON338. Eub338f and NON338 were hybridised with *E. coli* and sediment samples consecutively to check for non-specific binding.

2.2.7 - CARD-FISH Staining (A684r, Topamax 162F)

CARD-FISH staining was conducted using the probes A684r (5′-ACCA-GAAGTTCCACTCTC$_{biotin}$-3′; Sigma-Aldrich®) targeting AnAOB (Humbert *et al*., 2012) and Ntsp-amoA 162F (5′-GGATTTCTGGNTSGATTGGA$_{biotin}$-3′; Sigma-Aldrich®) targeting comammox bacteria (Fowler *et al*., 2018), reversed Eubacterial 16S rRNA control probe NON338 (5′-ACTCCTACGGGAGGCAGC-3′ $_{biotin}$; Wallner *et al*., 1993; ordered from Sigma-Aldrich®), all labelled with biotin. CARD-FISH staining was conducted using a modification of methods from Probandt *et al*. (2018). Fixed sediment (0.1 g wet weight) was permeabilised in 100 ng/µL lysozyme solution (Sigma-Aldrich®) for 80 min at room temperature. Sediment was inverted three times to mix. Sediment was then washed three times with 1x PBS. Following permeabilization, an endogenous biotin blocking kit (Molecular Probes E-21390; Invitrogen™) was used to remove endogenous biotin as per the manufacturer instructions, with 1 h selected for both incubation steps rather than 15-30 minutes. Manufacturer instructions found in appendix 3.2. Next, 3% (v/v) hydrogen peroxide solution was used to remove endogenous peroxidases from the sample at room temperature for 1 h. Samples were then washed three times with 1x PBS. For A684r attachment, samples were resuspended in 74 µL of 40% (v/v) hybridisation buffer (0.4 mL formamide, 0.1 mL of 300 mM Tris-HCl (pH 7.2) and 10 µL of 10% (w/v) SDS and 0.3 mL of molecular quality H_2O). For Ntsp-amoA attachment, samples were instead resuspended in 74 µL of 30% (v/v) hybridisation buffer (0.3 mL formamide, 0.1 mL of 300 mM Tris-HCl (pH 7.2), 10 µL of 10% (w/v) SDS and 0.4 mL of molecular quality H_2O). NON338 used an identical hybridisation buffer as the directly labelled version. After this, 10 µL of the respective fluorescent probe (conc = 5 ng/µL) was then added for a final probe concentration of 0.6 ng/µL. Samples were inverted three times to mix.

Sediment was then incubated overnight in a water bath at 37 °C. The following day, samples were washed three times with 1x PBS. HRP and tyramide was then attached using kits (Tyramide SuperBoost™ Kits with Alexa Fluor™ Tyramides; Invitrogen™) following manufacturer instructions. Any deviations from manufacturer instructions can be found in appendix 3.3. Tyramides were labelled with either Alexa Fluor488™ or Alexa Fluor555™. A 1 h incubation was chosen for HRP conjugation, and 3 min for tyramide addition. Finally, samples were washed three times with 1x PBS.

2.2.8 - CARD-FISH Controls and Optimizations

A lysozyme incubation series (with N = 3 for each timepoint) was run from 10 to 100 minutes to determine the relative strength of CARD-FISH probes to DAPI at different lysozyme incubation times. After, sediment samples were used to optimize formamide concentration in the hybridisation buffer. Non-specific binding was examined by staining *E. coli* with Ntsp-amoA and A684r.

2.2.9 - Image Acquisition and Processing

Samples were visualised using a Nikon A1R laser scanning confocal microscope with plan-apochromatic 20X and plan-apochromatic VC 60X objectives (Nikon Corporation). All figures shown in this thesis were captured using confocal microscopy. Stained samples were suspended in 1 mL of 1x PBS before plating into glass-bottom wells (35 mm Schott glass; Ibidi GMBH). DAPI and calcofluor white were excited using a 399.4 nm laser with emission captured between 450-500 nm, Acridine Orange and Alexa Fluor™ 488 were excited using a 488 nm laser with emission captured between 525-575 nm, and Alexa Fluor™555 was excited using a 560.9 nm laser with emission captured between 595-645 nm. Images at 60X were captured with a Nikon Ti-Z drive using 1.5 µm Z-steps. Cell size data was calculated using maximum intensity

projections in FIJI (Schindelin *et al*., 2012). Colony depths and cell-cell distances were measured in Nikon-Elements AR (Nikon Corporation).

2.2.10 - Fluorescein Negative Stain Technique for 3D Microtopography

Stained samples were examined using confocal fluorescence microscopy. Once the z-stack was captured, 24 µL of a 25 mg/µL fluorescein solution was pipetted off-centre into wells. A period of 15 min was given for fluorescein concentration to equalise throughout the well. A short 5s 488 nm laser firing was used to confirm fluorescence output, and thus concentration, had stabilised. After fluorescein concentration had equalised, a second z-stack of the same FOV was captured using a 488 nm laser with detection of 525-575 nm emission. NIS-elements AR was then used to produce a binary mask (i.e: negative impression - areas with no fluorescein fluorescence) of the sediment microtopology from this second z-stack. This binary mask was then superimposed onto the original z-stack, producing a 3D model containing both fluorophore and microtopography data. If the sample was not stained with dyes inside fluorescein's excitation and emission spectrum (Alexa Fluor488™ and acridine orange), both the dye stain and fluorescein negative stain were captured simultaneously.

2.2.11 - Fluorescein Negative Stain Optimization and Controls

Fluorescein staining controls were conducted on fluorescent plastic. A fluorescent plastic filter (Ted Pella Inc), with emittance of 540 nm, was broken into small, grain sized particles. Fluorescein was then added. Samples were imaged in 488 nm and 540 nm channels, and the fluorescein binary mask was compared to the fluorescent plastic outline.

The fluorescein negative stain was optimized for both concentration and imaging settings. Initial trials used a low (100 µL of a 2.5 mg/µL) fluorescein solution with high laser intensities (25-30%). When this failed to produce quality images, concentrations were increased to 24 µL of a 100 mg/µL solution with lower laser strengths (8-12%). This was later changed to the final concentration of 24 µL of a 25 mg/µL solution with laser strengths between 12-16%, depending on sample and magnification used.

2.2.12 – Colony Depth Measurements:

Colonies were examined in NIS-elements AR. Colonies were defined as either one contiguous area tagged with the relevant fluorophore, or a tight cluster of cells tagged with the relevant fluorophore. Once AnAOB and Eub338f positive colonies were identified, the nearby nominal surface of the sediment grain was determined by measuring the height of the surface (as determined from the fluorescein negative stain) in the Z-stack. If the colony appeared inside of a chasm, the height of both sides of the chasm wall were averaged to determine the nominal surface. Once this value was chosen, the beginning and end height of the colony were determined by measuring their height in the Z-stack. This could then be compared to the height of the nominal surface to determine depth. This was then repeated with calcofluor white and acridine orange-stained colonies. Some colonies were found detached from the sediment surface. These were discarded from all statistics as it was unsure if they represented free-floating colonies or colonies that had been detached during sample processing. All distance measurements were completed using tools in-built into NIS-elements AR.

2.3 – Results

2.3.2 – Trials with Directly Labelled Probes

Trials were conducted using the directly labelled probes Eub338f, NON338, AAO258f, and Amx368f. Eub338f showed counterstaining with DAPI and high signal strength versus background autofluorescence. NON338 showed no signs of counterstaining with Eub338f, suggesting that Eub338f/DAPI counterstained areas are not due to autofluorescence. Some autofluorescence was detected (see Fig. 2.2A) but was far weaker than Eub338f staining. As a result, directly labelled Eub338f was used through further trials as a Eubacterial counterstain for other probes (e.g: A684r; AnAOB), alongside DAPI. Both Eub338f and NON338 were found to require a hybridisation buffer with 40% formamide concentration.

AAO258f and Amx368f were found to require hybridisation buffers of 20% and 30% respectively. A further trial was conducted using AAO258f and Amx368f staining on sediment. AAO258f and Amx368f staining was weak compared to Eub338f and autofluorescence, resulting in a decision to trial CARD-FISH staining for AnAOB rather than continue with direct labelling. While this trial did find evidence of AOB and AnAOB co-staining in some areas, the weak fluorescent output from these probes leaves the possibility that this apparent co-staining is from autofluorescence.

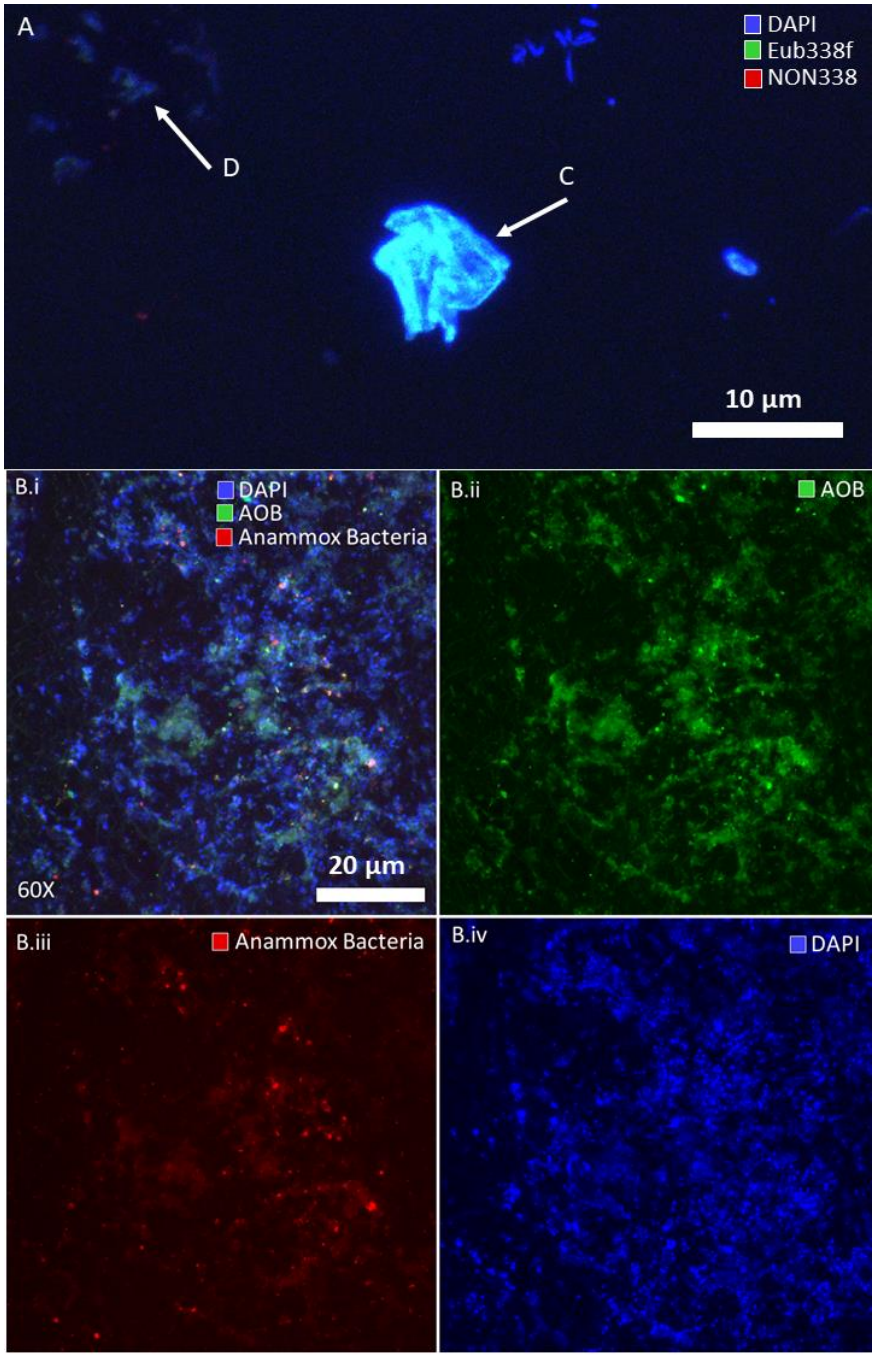

Fig. 2.2: Micrographs showing maximum intensity projections of the following: A = composite micrograph showing DAPI (blue; all DNA), Eub338f (green; Eubacterial 16S rRNA; direct labelling) and NON338 (red; reversed probe for Eub338f; direct labelling) labelling. Scale bar = 10 µm. B.i = DAPI (blue; all DNA), AAO258f (green; non-marine AOB 16S rRNA; direct labelling) and Amx368f (red; annamox bacteria 16S rRNA; direct labelling) labelling. Scale bar = 20 µm. B.ii – B.iv = separated channel micrographs of B.i. Images captured using Nikon A1R laser scanning confocal using 60X objective. Imaging channel settings found in methodology section 2.2.9 - Image Acquisition and Processing. Images analysed in NIS-elements AR. Data used in this figure derived from sample S3. C = Eubacterial biofilm stained with Eub338 and DAPI. D = Possible autofluorescence.

2.3.3 – Optimisation of CARD-FISH Method

The intensity of fluorescence from the NON338 probe relative to DAPI peaked after 80 minutes incubation in lysozyme. As a high level of autofluorescence had been noted during direct labelling attempts, 80 minutes was selected as the ideal incubation time to help increase accurate detection. Results shown in Fig. 2.3.

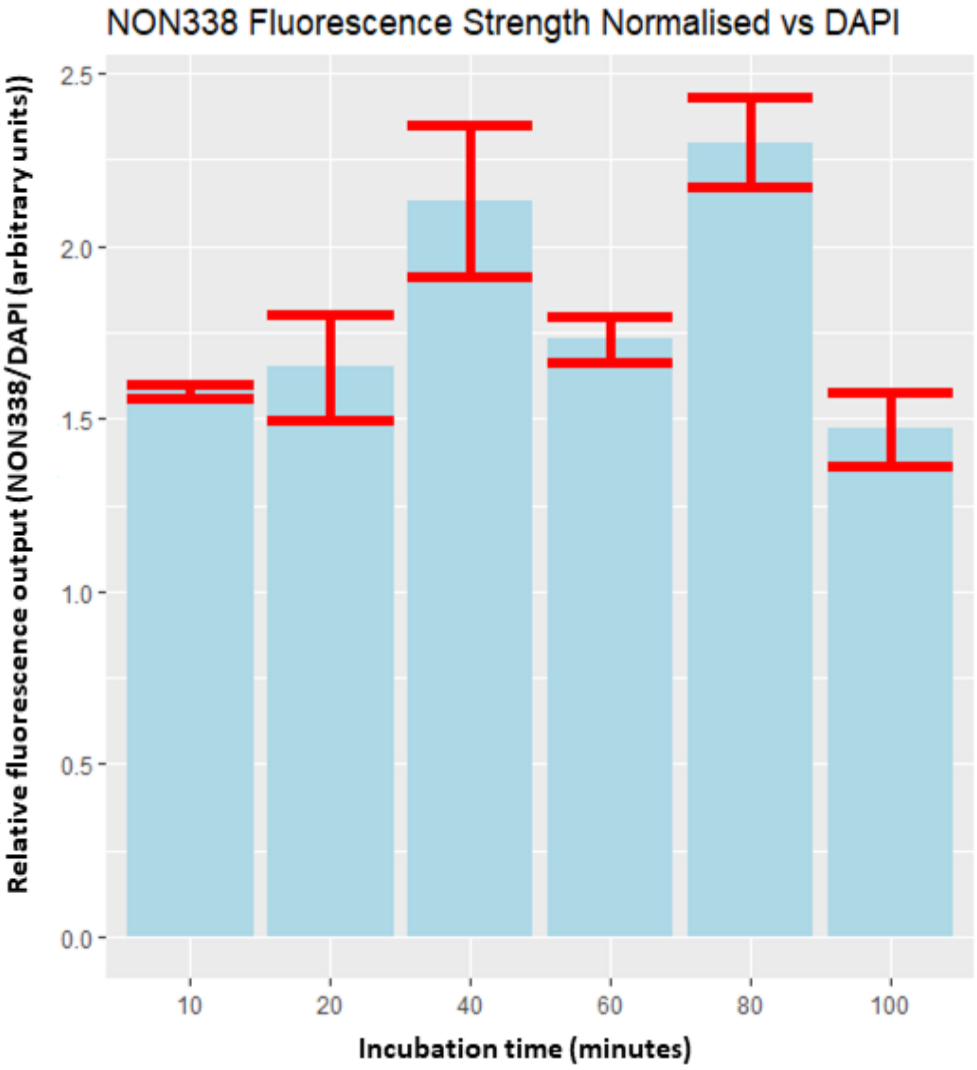

Fig 2.3: Lysozyme incubation effectiveness. Graph details the fluorescence output ratio between NON338 (CARD-FISH) and DAPI in *E. coli* cell culture over a lysozyme incubation time series of 10, 20 ,40 ,60 ,80 and 100 minutes. Results displayed in arbitrary units. Standard error bars shown in red. Three technical repeats for each timepoint. Images captured using Nikon A1R laser scanning confocal. DAPI was excited using a 399.4 nm laser with emission captured between 450-500 nm and NON338(Eubacteria; Alexa Fluor™555) was excited using a 560.9 nm laser with emission captured between 595-645 nm. Fluorescence output calculated using FIJI.

2.3.4 – Optimisation of Fluorescein Negative Stain

Initial trials conducted with low concentrations of fluorescein (100 µL of a 2.5 mg/µL solution) failed to produce quality images, with imaging artifacts commonly found on the grain surface, particularly at lower magnifications. The use of a large volume (100 µL) of fluorescein solution also often disturbed and moved sediment grains upon addition, preventing images from being correctly superimposed. Later, a much higher concentration (24 µL of a 100 mg/µL solution) was used successfully. A reduced volume reduced sediment grain movement significantly, allowing superposition of the sediment grain. Using a higher concentration combined with lower laser strength produced higher quality images without imaging artifacts. However, when fluorescent dyes outside of fluorescein's absorption/emission wavelengths (e.g: DAPI) were imaged simultaneously with fluorescein, this high concentration prevented dyes from being imaged correctly. As a result, a middling concentration was used (24 µL of a 25 mg/µL solution) which allowed imaging of both dyes like DAPI and fluorescein simultaneously. As a final confirmation test, this technique was used to examine fluorescent plastic fragments produced by shattering a microscope filter. The surface impression from the fluorescein negative stain closely matched that of the fluorescence from the plastic (see Fig. 2.4).

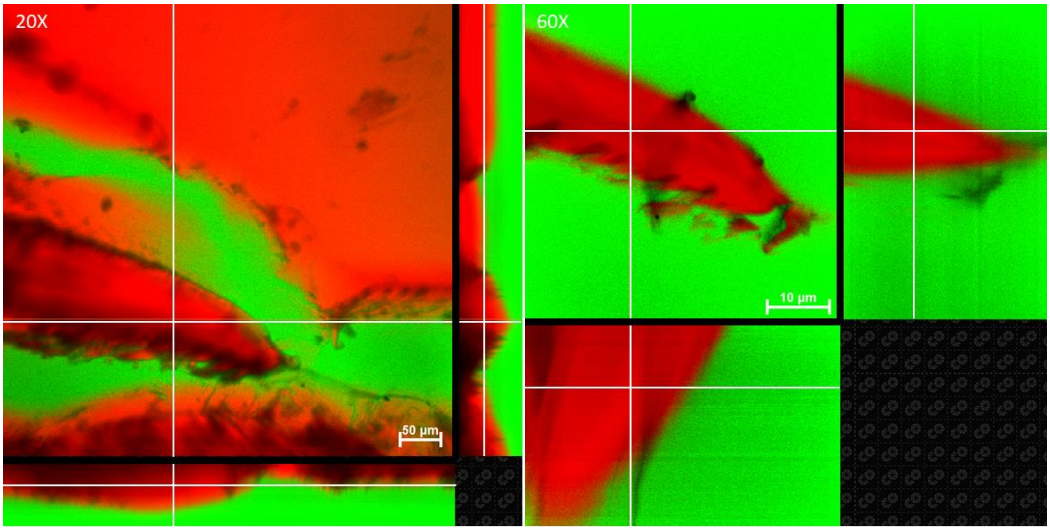

Fig. 2.4: Composite orthogonal projections of shattered fluorescent plastic filter and fluorescein staining. Taken with 20X and 60X obj. lenses. Images captured using Nikon A1R laser scanning confocal. Captured using 488 nm laser with detection of 525-575 nm and 560.9 nm laser with emission captured between 595-645 nm. Images analysed in NIS-elements AR.

2.3.1 - Fluorescein Negative Stains Show Variable Grain Microtopology

Microtopology varies over sediment grains. Most of the grain surface is convex and exposed, whereas other regions are sheltered by microtopographical features such as chasms and pits. Chasms varying greatly in size and depth, with chasm floors consisting of a fractal network of subchasms and pitted areas (see Fig. 2.5). The chasm shown in Fig. 2.5 is approximately 60 µm below the nominal surface at its deepest point.

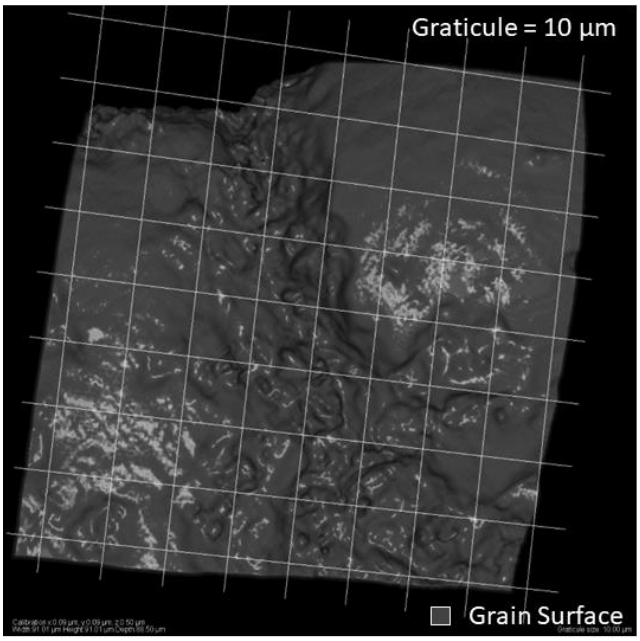

Fig. 2.5: 3D model of sand grain at 60X obj. produced using fluorescein negative staining. Graticule = 10 µm. A digital light source was used to produce shadowed and bright areas on the model. Image captured using Nikon A1R laser scanning confocal. Captured using 488 nm laser with detection of 525-575 nm. Images analysed in NIS-elements AR. Greensand sample taken from S3.

2.3.2 - Epilithic and Chasmoendolithic Eubacterial Colonies

In all stained samples mentioned in this thesis, and based on qualitative analysis, Eubacterial colonies were found exclusively in areas sheltered by microtopography. Chasms on the grain surface were heavily colonised by Eubacterial cells, although most cells remained in epilithic biofilms. Examples of this can be found in Fig. 2.10. Convex and exposed areas were generally barren of cells, showing little staining with either DAPI or Eub338f.

2.3.3 - AnAOB as Chasmoendoliths

Chasmoendolithic AnAOB form colonies in chasms on the grain surface (see Fig. 2.6A-C). The microtopology of these sites, narrow openings, and presence of AnAOB suggest that these chasms are anoxic microsites in otherwise oxic sediment. Rarely (10.7% of colonies), epilithic AnAOB colonies were detected. My data shows that

epilithic AnAOB colonies on the sediment surface are surrounded by other microorganisms, which stain with a mixture of either DAPI or Eub338f + DAPI, suggesting that AnAOB can form biofilms with other Eubacteria and either Archaea, Eukaryotes or both. Some chasmoendolithic AnAOB colonies extend slightly above the surface. These partially chasmoendolithic AnAOB colonies extend an average of 1.6 μm above the surface and are capped by either DAPI or Eub338f stained cells, in a manner identical to epilithic colonies. A ‘capped’ chasmoendolithic colony is shown in Fig. 2.6D. The midpoint of AnAOB colonies ranged from 0.41 μm above to 4.9 μm below the sediment grain surface. In comparison, the midpoint of Eubacterial colonies in general (and excluding colonies containing AnAOB) ranged from 1.6 μm above to 2.1 μm below the sediment grain surface. A one-way ANOVA test was performed and revealed a statistically significant difference between Eubacterial and AnAOB colonies overall (F = 8.906, p = 0.00435). A Tukey post-hoc test was conducted and also showed similar significance p adj = 0.00435). After this, a further one-way ANOVA was used to examine the difference between AnAOB in sand and in chalk, with no significant difference in depth detected (F = 0.29, p = 0.595). Full depth statistics are displayed in Fig. 2.7. Out of AnAOB colonies discovered, 22/28 (78.6%) were classified as completely chasmoendolithic, 3/28 (10.7%) were classified as partially chasmoendolithic and 3/28 (10.7%) as epilithic. In regions containing AnAOB colonies, filamentous Eubacterial colonies were relatively common – accounting for 13.8% of Eubacterial colonies in surrounding regions. Filamentous Eubacterial colonies consisted of both monofilament and multifilament morphologies. Dataset for colony type and filamentous colonies identical to that of Fig. 2.7. Colony type and filamentous colony status designated qualitatively.

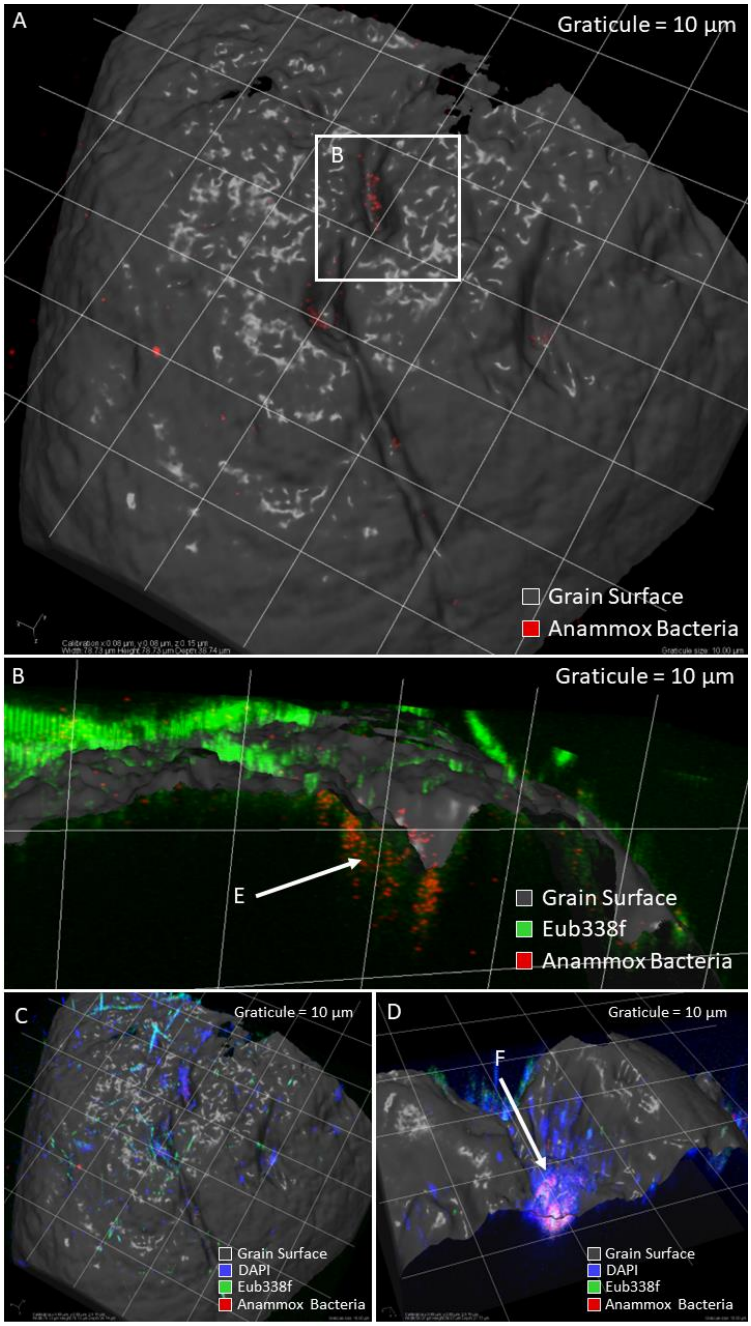

Fig. 2.6: 3D models of sediment grains showing various types and sizes of AnAOB colony. Sediment stained with DAPI (blue, all DNA), Eub338f (green, Eubacteria 16S rRNA probe, direct labelling) and A684r (red, AnAOB 16S rRNA; CARD-FISH). Grain surface impression produced by fluorescein negative staining. All micrographs taken with 60X objective magnification. Grey represents the grain surface. A digital light source was used to produce shadowed and bright areas on the model. Graticule = 10 µm. A = micrograph showing chasmoendolithic anammox colony, image captured from sample C1. B = micrograph showing cutaway section of colony in A. C = identical to micrograph A but displaying DAPI and Eub338f staining. D = example of partially chasmondolithic anammox colony, image captured from sample C2. Images captured using Nikon A1R laser scanning confocal. Imaging channel settings found in methodology section 2.2.9 - Image Acquisition and Processing. E = Chasmoendolithic AnAOB colony. F = Partially chasmoendolithic AnAOB colony.

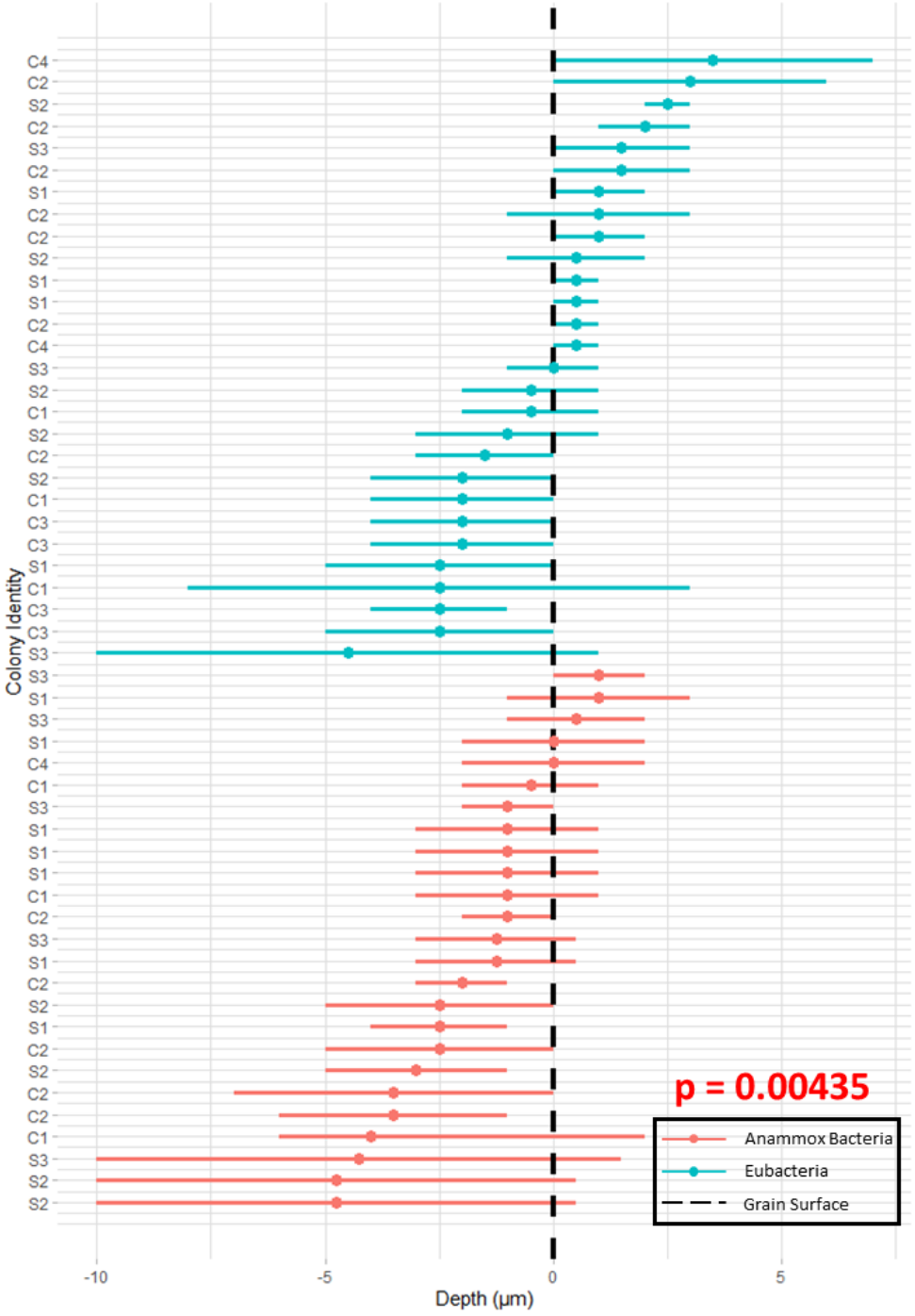

Fig. 2.7: Depths of AnAOB colonies and Eubacteria colonies (not including colonies containing AnAOB). Data depicts beginning and end of colonies in relation to the grain nominal surface. AnAOB colonies are displayed in red, Eubacterial in cyan. Sediment surface is marked with dashed line. Significant difference detected between AnAOB and Eubacteria using ANOVA statistical test (p = 0.00435). Data gathered from samples C1, C2, C3, C4, S1, S2 and S3. Data captured using Nikon A1R laser scanning confocal and processed in NIS-elements AR. Eub338(Eubacteria; Alexa Fluor™ 488) was exited using a 488 nm laser with emission captured between 525-575 nm, and A684r (AnAOB; Alexa Fluor™555; CARD-FISH) was excited using a 560.9 nm laser with emission captured between 595-645 nm.

2.3.4 - AnAOB and Comammox Bacteria

Data was collected from samples C1, C2, C4, S1, S2, and S3. Distances between AnAOB and comammox bacteria varied greatly (mean distance = 14.5 ±20.9 µm, range = 129.26 µm). It was found that 35.2% of AnAOB were within 1 µm or less of an a comammox bacterial cell/colony. A histogram demonstrating AnAOB/comammox bacteria distance distribution can be found in Fig. 2.8. Given the amount of sediment surface colonised (mean 22.3 ±8.9% of the grain surface), and low *hzo* abundance (Lansdown *et al.*, 2016), it is likely that some association exists between these N-cycle groups.

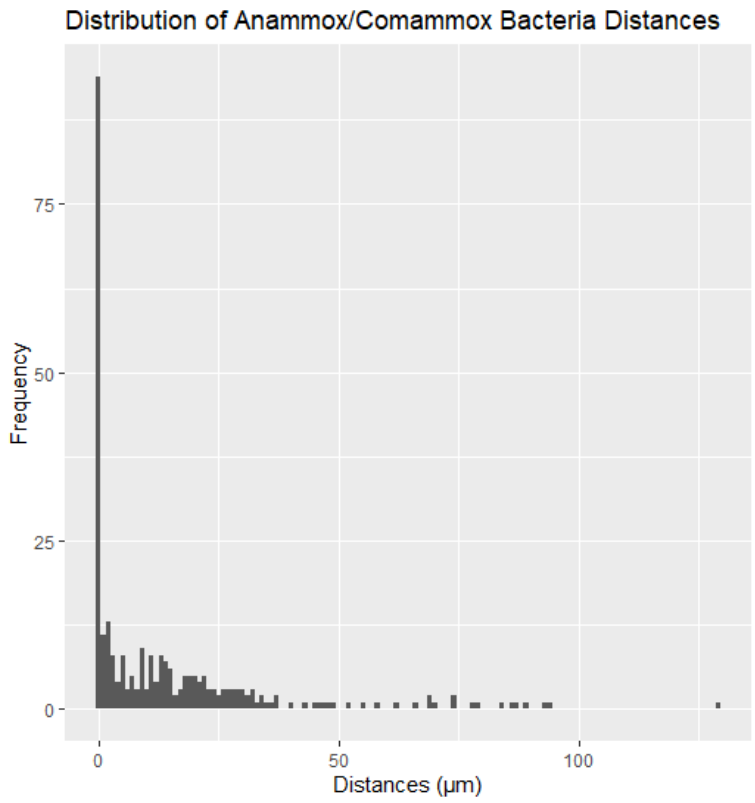

Fig. 2.8: Histogram showing distribution of the distances between AnAOB and the nearest comammox bacteria. Bin width = 1 µm. Data collected from samples C1, C2, C4, S1, S2 and S3. Data captured using Nikon A1R laser scanning confocal and processed in NIS elements. DAPI was excited using a 399.4 nm laser with emission captured between 450-500 nm, Ntsp-amoA (comammox bacteria; Alexa Fluor™ 488; CARD-FISH) was exited using a 488 nm laser with emission captured between 525-575 nm, and A684r (AnAOB; Alexa Fluor™555; CARD-FISH) was excited using a 560.9 nm laser with emission captured between 595-645 nm.

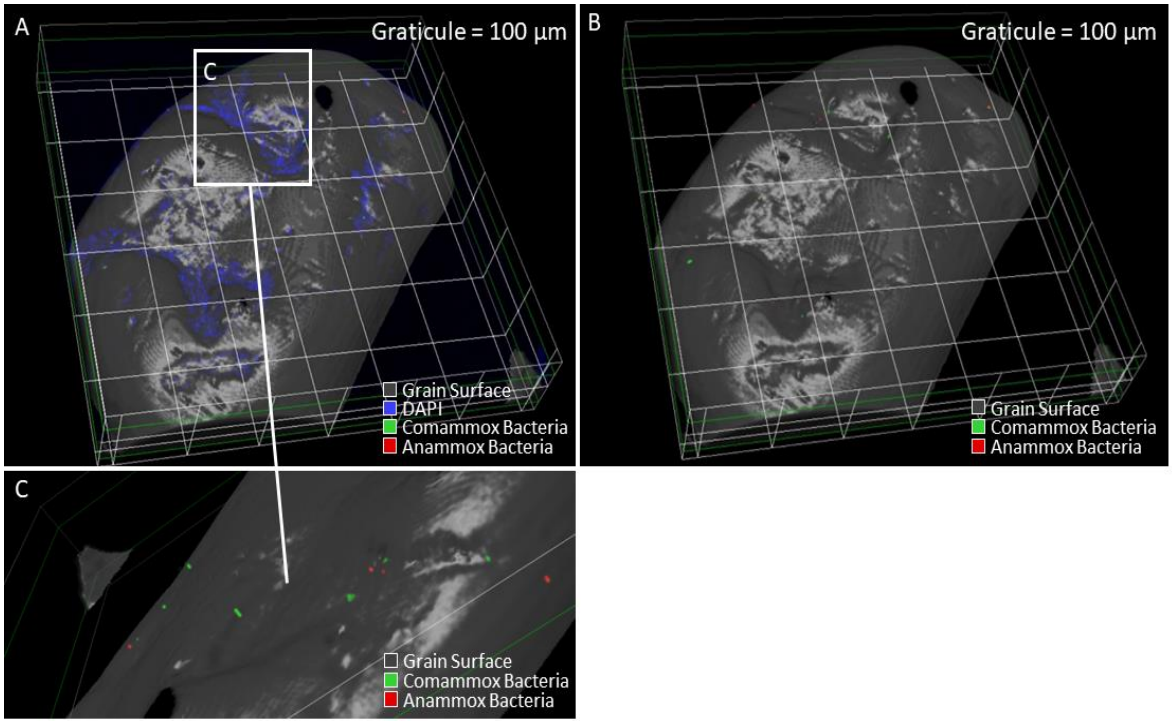

Fig. 2.9: 3D representations of a sediment grain showing A = DAPI (blue; all DNA), Ntsp-amoA 162f (green; comammox bacteria *amoA* gene) and A684r (red; AnAOB 16S rRNA) staining. B&C = Ntsp-amoA 162f (green; comammox bacteria *amour* gene) and A684r (red; AnAOB 16S rRNA) staining. Graticule = 100 µm. Graticule removed from C for image clarity. Grain surface impression produced by fluorescein negative staining. A digital light source was used to produce shadowed and bright areas on the model. Image taken with a Nikon A1R laser scanning confocal using a 20 X objective. DAPI was excited using a 399.4 nm laser with emission captured between 450-500 nm, Ntsp-amoA (comammox bacteria; Alexa Fluor™ 488; CARD-FISH) was exited using a 488 nm laser with emission captured between 525-575 nm, and A684r (AnAOB; Alexa Fluor™555; CARD-FISH) was excited using a 560.9 nm laser with emission captured between 595-645 nm. Images analysed in NIS-elements AR. Images above come from sample C2.

2.3.5 - Fungi and Algae Distribution and Characteristics

A comparison of calcofluor white (fungi and algae) stained cells versus acridine orange-stained cells (all DNA; analysis excluding cells showing calcofluor white co-localisation) found calcofluor white-stained cells to have an average depth of 0.26 µm below the grain surface. In comparison, acridine orange-stained cells had an average depth of 0.62 µm above the grain surface. A one-way ANOVA test was performed and revealed a statistically significant difference between fungal/algal and non-fungal / algal colonies (F = 12.73, p = 0.000569). Calcofluor white-stained cells are lightly

'burrowed' into the grain surface, with colonies/individual cells extending slightly past the surface. An example of this can be found in Fig. 2.10.

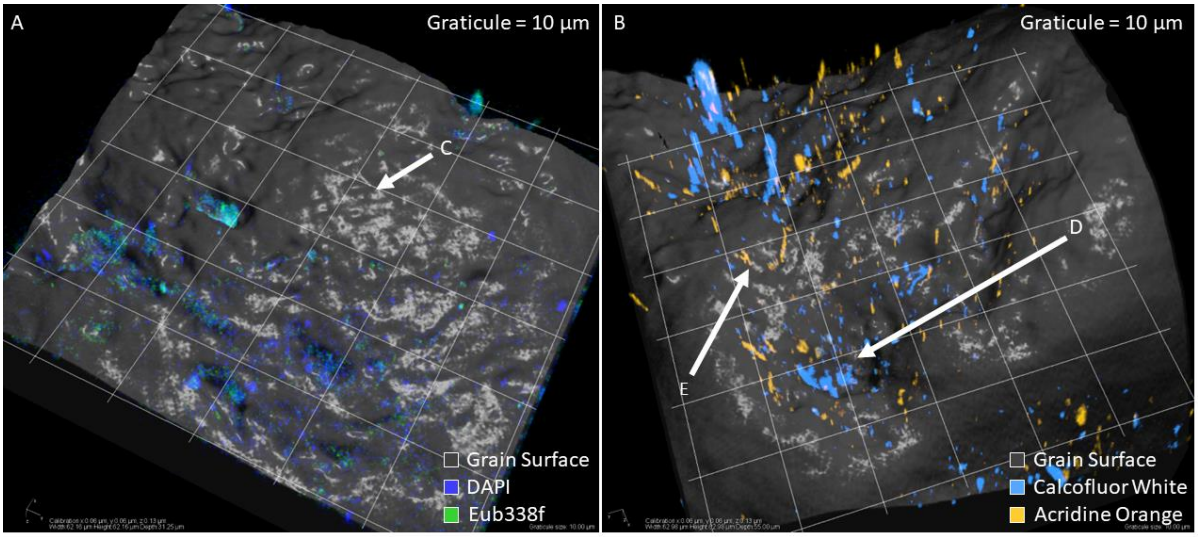

Fig. 2.10: 3D representation of sediment grain surface showing A = DAPI (all DNA, blue) and Eub338f (eubacteria 16S rRNA probe, green) staining. Image captured from sample C3. B = calcofluor white (fungal and algal cell walls, light blue) and acridine orange (all DNA, orange) staining. Image captured from sample C1. Grain surface impression produced by fluorescein negative staining. A digital light source was used to produce shadowed and bright areas on the model. Graticule = 10 µm. Areas of interest are highlighted. Images taken Nikon A1R laser scanning confocal. Images analysed in NIS-elements AR. 60X obj. mag. Calcofluor White was excited using a 399.4 nm laser with emission captured between 450-500 nm and Acridine Orange (All DNA and RNA) was exited using a 488 nm laser with emission captured between 525-575 nm. C = Barren, convex area. D = Chasm containing fungi/algae. E = epilithic microbes (unknown group).

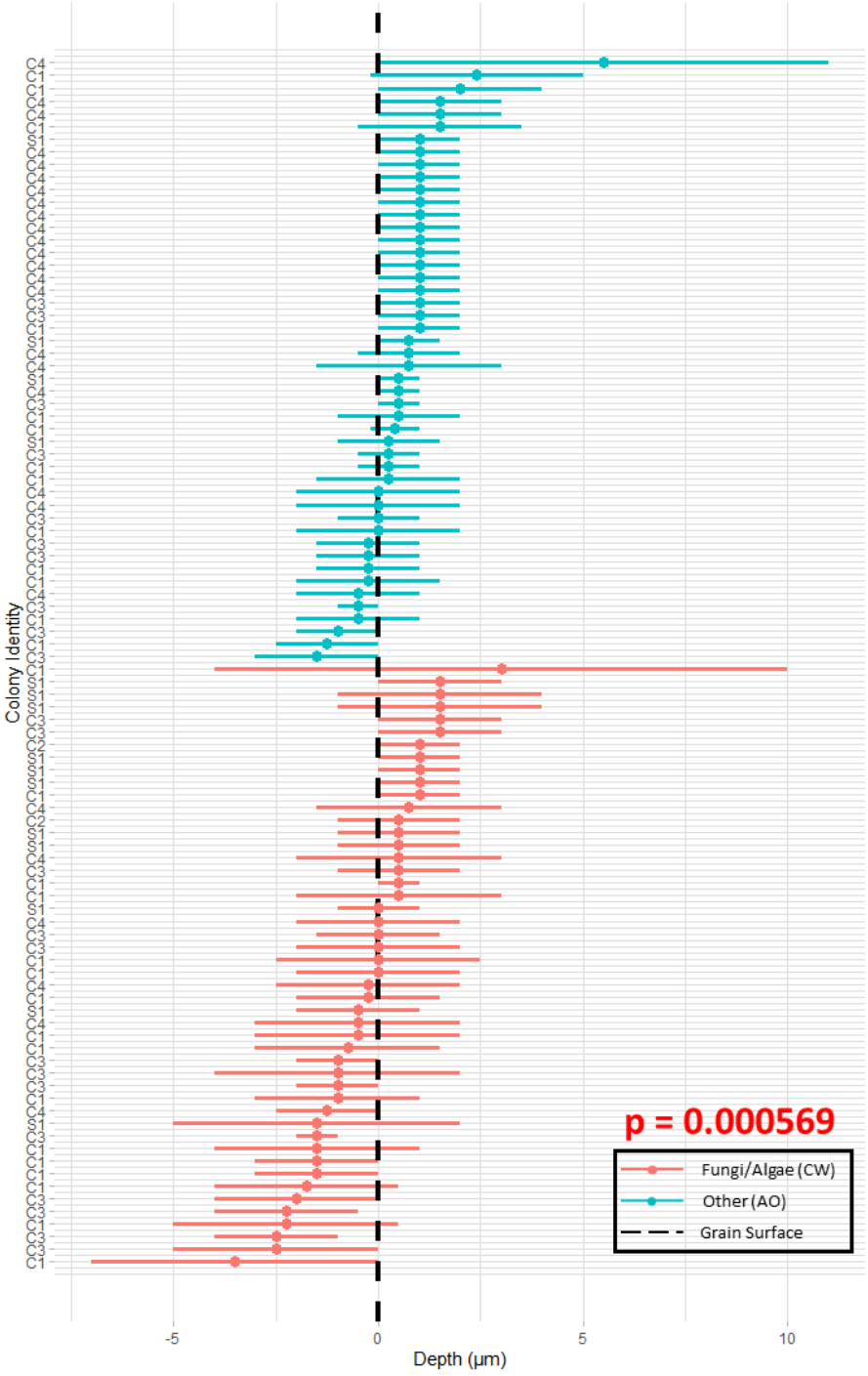

Fig. 2.11: Depths of fungal/algal (calcofluor white stained) colonies versus other colonies (acridine orange stained). Data depicts beginning and end of colonies in relation to the grain nominal surface. Fungal/algal colonies are displayed in red, other in cyan. Sediment surface is marked with dashed line. Significant difference detected between colony types using ANOVA statistical test (p = 0.000569). Data collected from samples C1, C2, C3, C4, S1. Data captured using Nikon A1R laser scanning confocal and processed in NIS elements. Calcofluor White was excited using a 399.4 nm laser with emission captured between 450-500 nm and Acridine Orange (All DNA and RNA) was exited using a 488 nm laser with emission captured between 525-575 nm.

2.4 - Discussion

My research shows that most AnAOB are chasmoendoliths. Chasms inhabited by AnAOB could have a have declining oxygen gradient that yields anoxic microsites. The discovery of DAPI/Eub338f stained caps on chasmoendolithic colonies further suggests that various bacterial and non-bacterial species can influence this oxygen gradient. AnAOB, an anaerobic group, may colonise and use these presumed anoxic microsites for protection from molecular oxygen. Cell-cell distance data further suggests comammox bacteria as candidates for 'colony-cap' species, matching results seen in bioreactors (Hu *et al*., 2013; Cao *et al*., 2017; Gottshall *et al*., 2021). My discovery of chasmoendolithic AnAOB, AnAOB-comammox colocalization in sediments and non-bacterial 'colony-caps' on AnAOB colonies, suggests that numerous microbial group-microtopology interactions may contribute to the role of AnAOB in oxic sediments, with the closest analogous environmental biology research studying AnAOB interactions on flocs in OMZs (Woebken *et al*., 2007).

Some substrata for colony attachment are inorganic, meaning the substrata cannot be mapped using fluorescent signalling. This has made it difficult to determine the interaction between biofilms and their substrata. My discovery of anoxic microsites containing AnAOB would not have been possible without the development of my novel fluorescein negative-stain technique. This technique solves an ongoing problem in biofilm-substrata interaction studies. While having inferior resolution to SEM microscopy, the ability to combine microtopology with fluorophore tagging makes this a powerful technique for studies of biofilm-substratum interaction. Previous studies examining the possibility of anoxic microsites within other sediment types have used other techniques such as radiological tagging (Jahnke, 1985; Rao *et al*., 2007; Cook *et al*., 2017) and optode (microelectrode) imaging systems (Keilluweit *et al*., 2018).

The majority of AnAOB were found in deep chasms on the grain surface. Many chasmoendolithic AnAOB colonies were surrounded on their surface by non-anammox cells – referred to in this thesis as ‘colony-caps’. Colony-caps sometimes consisted purely of DAPI stained cells, with little or no Eub338f staining present, suggesting a largely non-eubacterial make-up. It should be noted that Eub338f may have difficulty diffusing into colonies and anoxic microsites, possibly explaining this result. Ammonia oxidising archaea (AOA) are a possible candidate for non-bacterial colony-caps and can readily supply nitrite for the metabolism of AnAOB as this relationship can exist under oxygen stratification (Straka *et al*., 2019).

My results show some association between AnAOB and comammox bacteria exists in sediments, with comammox bacteria being a ‘colony-cap’ group. Recent research yields some insight into potential symbiosis. Gottshall *et al.* (2021) discovered that comammox bacteria are capable of supplying nitrite to AnAOB. This relationship is similar to that between AnAOB and AOB found in bioreactors – comammox bacteria supplying nitrite and protection from molecular oxygen. Gottshall *et al.* (2021) experimented with comammox and AnAOB embedded gel-beads to prove this concept, rather than a natural system, but my research shows this relationship may also existing in sediments. Furthermore, as discussed above, many chasmoendolithic AnAOB colonies show little or no Eub338f staining in their protective ‘caps’, suggesting that non-bacterial group(s), perhaps AOA, can provide a similar benefit.

The endolithic locations of fungi and algae seen in this study are backed up by previous research (Perkins and Halsey, 1971). Fungi, algae and lichen – all stained by calcofluor white – are important for euendolithic activity in sediments (Wierzchos *et al*., 2011). While the results of this thesis regarding fungi and algae are not novel, it demonstrates the accuracy of the fluorescein negative-stain technique developed for

this study. Correctly identifying groups with known endolithic members (fungi, algae) as endolithic suggests that my negative-stain technique, and subsequent method of measuring depth, are working correctly.

One possible historical interaction between AnAOB and other groups lies in the creation of chasms. Some endolithic organisms are classified as euendolithic - capable of engineering favourable environments in sediments (Wierzchos *et al*., 2011). Euendolithic cyanobacteria are responsible for the majority of euendolithic activity in carbonate rocks, such as limestone and chalk. Initial environmental engineering by cyanobacteria is conducted by members of the order Pleurocapsales, with further chasm formation by other species such as *Leptolyngbya terebransi* and *Mastigocoleus testarum* (Ramírez-Reinat and Garcia-Pichel, 2012; Roush and Garcia-Pichel, 2020). Rather than being euendolithic, AnAOB may instead colonise chasms already formed by these euendolithic cyanobacterial groups. As cyanobacteria are unlikely to survive in anoxic conditions, this relationship may only exist historically. Another possible interaction is between AnAOB and euendolithic fungi or algae. However, endolithic fungi/algae colonies found in this study were significantly shallower than the chasmoendolithic AnAOB colonies found, suggesting a third group (i.e: euendolithic cyanobacteria) is still involved. If a relationship between AnAOB and euendolithic fungi/algae does exist, it may have been hidden by methodological flaws in this study – the incubation time used for calcofluor white (CW) was significantly shorter than for FISH probes and DAPI – a decision chosen due to the strong staining produced by CW. This shorter incubation time may have prevented CW from diffusing into narrow cracks in a similar manner to fluorescein, causing fungi/algal colonies to ‘cut-off’ before their actual end. Further attempts to examine commensalism between AnAOB and fungi/algae should make use of longer CW incubation times.

Fluorescein staining matched up closely with fluorescence from fluorescent plastic, suggesting a high level of fidelity to the true surface. The 3D topology models produced by fluorescein have a high resolution – around ~300 nm - close to the expected resolution given the emittance wavelength of fluorescein (521 nm). Grain microtopology seen via fluorescein imaging is identical to that seen from scanning electron microscope (SEM) studies of sand grains, further supporting the accuracy of the technique (Beeftink and Staugaard, 1986). One notable issue is the inability to detect chasms past a certain depth – causing an effect where some chasmoendolithic colonies appear to penetrate through the grain surface. An explanation for this phenomenon is that fluorescein has low photostability and may have difficulty diffusing into such narrow chasms due to a lower surface area for diffusion to occur over, resulting in fluorescein loss to photobleaching being higher than the replacement rate of incoming molecules dissolved in the PBS used to suspend sediment. This may mimic the development of anoxic sites – the rate of incoming molecular oxygen being lower than the rate of use by respiring aerobic microbes near the top of anoxic indents.

The use of AnAOB is widespread in wastewater treatment. Anammox-based bioreactors are more efficient than nitrification/denitrification-based systems, with near elimination of carbon demand (Wett, 2007), and a 90% reduction in excessive sludge (Schaubroeck *et al*., 2015). Furthermore, carbon-decoupling means that anammox-based bioreactors have the potential to be energy positive - effluent can be further used in biogas generation, subsequently reducing treatment costs (Siegrist *et al*., 2008). In CANON (Complete Autotrophic Nitrogen Removal Over Nitrite) bioreactors, AnAOB form flocs with AOB, consisting of an anoxic core region of AnAOB and an oxic outer layer of AOB (Vlaeminck *et al*., 2008; Hu *et al*., 2013). In oxic sediments analysed in this study, this may not be the case – it is possible that AnAOB are instead

protected from molecular oxygen by anoxic microsites in chasms. This opens interesting possibilities for novel and improved bioreactor designs. It must be noted that in AOB/AnAOB flocs, AOB do not always cover the entire anoxic core (Vlaeminck *et al*., 2008), which may impact oxygen tolerance.

Interest has grown in the use of macro- and microporous carriers in AnAOB based bioreactors (Ahmad *et al*., 2017; Yang *et al*., 2021). Yang *et al*. (2021) found that microporous carriers showed greater biofilm thickness and enhanced nitrogen removal over microporous carriers. AnAOB population numbers and diversity were similar across both macro- and microporous carriers. AOB populations, in comparison, were two-fold higher in the macroporous carrier. Microporous carriers had large anoxic zones in deeper layers of the carrier. This may suggest that AnAOB are relying on anoxic microsites within microporous carriers in a system analogous to my suggested mechanism for AnAOB survival in oxic sediments, rather than on a relationship with AOB. This mechanism is further backed up by research from Ahmad *et al*. (2017) showing that AnAOB congregate in the centre of carriers. Interest has also grown in the use of AnAOB concurrently with porous microbeads (Bae *et al*., 2015; Ali *et al*., 2016). Research shows that systems based around porous microbeads have high populations of anammox bacteria (Bae *et al*., 2015). Furthermore, Ali *et al*. (2016) shows a similar mechanism in porous microbeads, with AnAOB being located in central zones. It is possible that anoxic microsites in sediment grains act in a similar fashion to porous carriers and porous microbeads – supporting the structure of nitrogen cycling microbial communities.

The primary limitation of this research is the methodology behind colony depth calculations. Depth calculations, and associated colony counts, were conducted by hand rather than automatically due to a lack of available software. This introduces the

potential for human error into my datasets. Furthermore, rather than counting the depth of each individual cell, cells were grouped into colonies for ease of counting. Colonies also varied in size. Size data was collected alongside depth data, but the numbers quoted in this research are unweighted averages that do not take into account colony size. Notably, chasmoendolithic AnAOB colonies were far larger than epilithic. This makes the depth stats calculated for this research an approximation rather than absolute number, with AnAOB possibly being more chasmoendolithic than suggested by my presented data. This, combined with the time taken to image each image set (with an individual confocal stack often taking over an hour to image) and rarity of AnAOB colonies, reduced the size of my datasets. It is best to bear in mind that this data was collected using a novel, and experimental, technique, and that future work may solve this problem by the development of supporting software. The lack of steps taken to prevent contamination or manage the oxic/anoxic environment pre-fixation may affect the results of this research. Lastly, colonies were occasionally found detached from the sediment surface. This was more common with calcofluor white / acridine orange staining, with all examples being discarded from statistics shown in this thesis. This was possibly caused by the lack of fixation. This could produce a potential bias towards chasmoendoliths as they may be less likely to detach during sample preparation.

Future work on AnAOB interactions in sediment should focus on further co-localisation studies between AnAOB and other N-cycle groups, especially AOB. This could be combined with our fluorescein negative staining technique to develop a model of interactions. It is possible that anoxic microsites in sediments act in a similar way to microporous carriers (Ahmad *et al*., 2017; Yang *et al*., 2021). My research could be further combined with optode- or radiological tagging-based experiments to determine

if chasms in riverine sediment are in fact anoxic like anoxic microsites found in other sediments (Jahnke, 1985; Rao *et al*., 2007; Cook *et al*., 2017; Keilluweit *et al*., 2018). The development of software for colony depth measurement would aid future research by allowing larger scale, more accurate data accumulation.

In conclusion, previous research on AnAOB in sediments has focused on environmental genetics (gene abundances) and nutrient flows, with the role played by AnAOB in oxic sediments only discovered within the last half-decade (Lansdown *et al*., 2016). Microscopy co-localisation studies have largely used engineered environments in bioreactors, with a model of AOB/AnAOB symbiosis being developed, with further and more recent research exploring the possibility of anoxic microsites in engineered carriers. My results suggest interactions between AnAOB, other microbial groups, and anoxic sites produced by sediment microtopology. The mechanism behind chasm colonisation by AnAOB is unknown, and AnAOB relationships to euendolithic groups could be a direction of future research. Further co-localisation studies between AnAOB and other N-cycle groups may help build a full model of the anammox process in oxic sediments. Theoretical bioreactor designs utilizing AnAOB/comammox bacteria symbiosis are very recent (Gottshall *et al*., 2021), yet this relationship is possibly seen via co-localisation in sediments, so a more complete knowledge of AnAOB co-localisations can lead to other theoretical designs being tested, including those utilizing anoxic microsites. The fluorescein negative staining technique developed during this research has many potential applications in biofilms studies, studies of colony adhesion to substratum, and research into lithic microorganisms.

Appendix A - 3 – Supplementary Information for Chapter 2

3.1 - A684r and Ntsp-amoA Controls

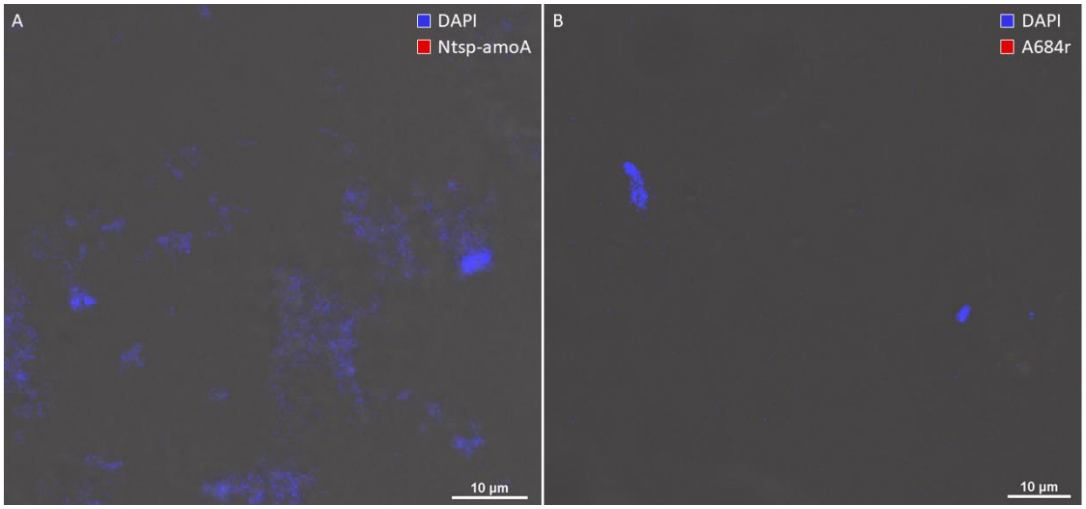

Fig. 3.1: Maximum intensity projection micrographs showing DAPI and CARD-FISH of A = Ntsp-amoA or B = A684r staining of *E. coli*. Designed as negative control. Taken with 20X obj. lens. Conducted with 3 biological repeats for each control set. CARD-FISH Staining.

3.2 – Manufacturer Instructions for Molecular Probes E-21390:

Fix and permeabilise cells according to established procedures. Apply one or two drops of the streptavidin solution to cells or tissue and incubate for 15-30[1] minutes at room temperature or 37 °C in a humid environment[2]. Rinse thoroughly with a buffer[3] (e.g: PBS). Add 1-2 drops of the biotin reagent and incubate for 15-30 minutes at room temperature or 37 °C in a humid environment. Rinse thoroughly with buffer, then proceed with established labelling procedures.

[1]Study conducted using 1 h incubation times rather than 15-30 minutes.

[2]Study conducted using 2 drops (~100 µl) of both streptavidin and biotin solutions.

[3]Study used 1x PBS as preferred wash buffer.

3.3 – Manufacturer Instructions for Tyramide SuperBoost™ Kits with Alexa Fluor™ Tyramides:

If needed, quench endogenous peroxidase activity using 3% hydrogen peroxidase solution. Rinse the cells thoroughly three times with 1x PBS at room temperature. If needed, block endogenous biotin with kit. Rinse the cells thoroughly three times with 1x PBS before continuing[1]. Add 2-4 drops (~100-150 µl) of blocking buffer[2] to the sample and incubate for 60 minutes at room temperature. Label the cells or tissue with biotin conjugated antibody[3]. For FISH, incubate the DNA/RNA probe according to manufacturer instructions. Rinse the cells or tissue for 10 minutes with 1x PBS at room temperature. Add 2-3 drops (~100-150 µl) of HRP conjugated streptavidin to the cells or tissue and incubate for 60 minutes at room temperature. Rinse the cells or tissue for 10 minutes with 1x PBS at room temperature. Prepare tyramide working solution and apply 100 µl[4] to cells or tissue and incubate for 2-10 minutes at room temperature[5]. Apply 100 µl of reaction stop solution. Lastly, rinse the cells or tissue three times in 1x PBS.

[1]As described in section 2.2 – Materials and Methods.

[2]This study used 2 drops (~100 µl) of blocking buffer and HRP conjugated streptavidin.

[3]As described in section 2.2 – Materials and Methods.

[4]This study used 76 µl of tyramide and reaction stop solutions.

[5]Three minutes selected. Tubes were inverted each minute during procedure.

4 - Appendix B – Microscopic Investigation of Dust Particles

4.1 – Introduction

The microbial community in house dust has been well studied using genetic based techniques. The makeup of the microbial community in dust shows core consistency. *Penicillium*, *Aspergillus* and *Cladosporium* are among the most dominant fungal groups in house dust (Rintala *et al*., 2012). The prokaryotic community is primarily formed from gram positive bacterium, with *Acinetobacter*, *Massalia, Rubellimicrobium*, *Sphingomonas* and *Staphylococcus* being ubiquitous across all house dusts (Thompson *et al*., 2021). Both the fungal and prokaryotic community are known to vary across climates (Amend *et al*., 2010; Thompson *et al*., 2021). There is evidence that the microbial community in dust can be disease causing (Birzele *et al*., 2017).

No fluorescence microscopy studies have been conducted on house dust (via Google Scholar & Pubmed search in 2021), Alongside genetic based techniques (qPCR, sequencing), FISH-based microscopy is becoming a common technique in examining sediments, with the first sediment grain-based study being conducted recently (Probandt *et al*., 2018). This research opened many possibilities in microbial ecology studies and was the inspiration for the primary research conducted in this thesis. It is my belief that, if FISH-based microscopy can be similarly applied to house dust samples, it may lead to a greater understanding of the microbial dust community. As a result, we have conducted confocal fluorescence microscopy research into the feasibility of this approach using a fungal and general DNA dye as a proof for future grant applications.

4.2 – Methods

Preliminary analysis was conducted using calcofluor white (Sigma-Aldrich®) and acridine orange (Invitrogen™). Staining methods and microscope setup were as previously described (see Sections 2.2.4 and 2.2.9). Dust was collected across various houses in Colchester, UK.

4.3 – Results

Based on autofluorescence and structure, dust particles consisted of clumped organic matter interwoven with unidentified fibres (see Fig. 4.1). Organic material autofluoresced strongly in the 450 nm to 500 nm and 595-645 nm bands. Overall, fibres showed autofluorescence occurred across all bands, but each individual fibre would only autofluoresce in a particular band. Acridine orange (AO) and calcofluor white (CW) aspecifically bound to fibres. This effect was stronger for CW. AO staining detected small coccus cells surrounding dust particles, but staining was unable to determine if similar cells could be found in dust particles due to strong autofluorescence. Coccus microbes detected by AO staining did not counterstain with calcofluor white. No CW staining was detected outside of dust particles, yet strong CW staining was detected within them. As small/frayed fibres have a similar filamentous morphology to hyphae, it is unknown if this staining was due to fungal presence or aspecific binding. Numerous ~30 µm long structures were detected. These structures auto fluoresced weakly in the 450 nm to 500 nm band and were identified as keratinocytes. Keratinocytes were usually found in association with dust particles.

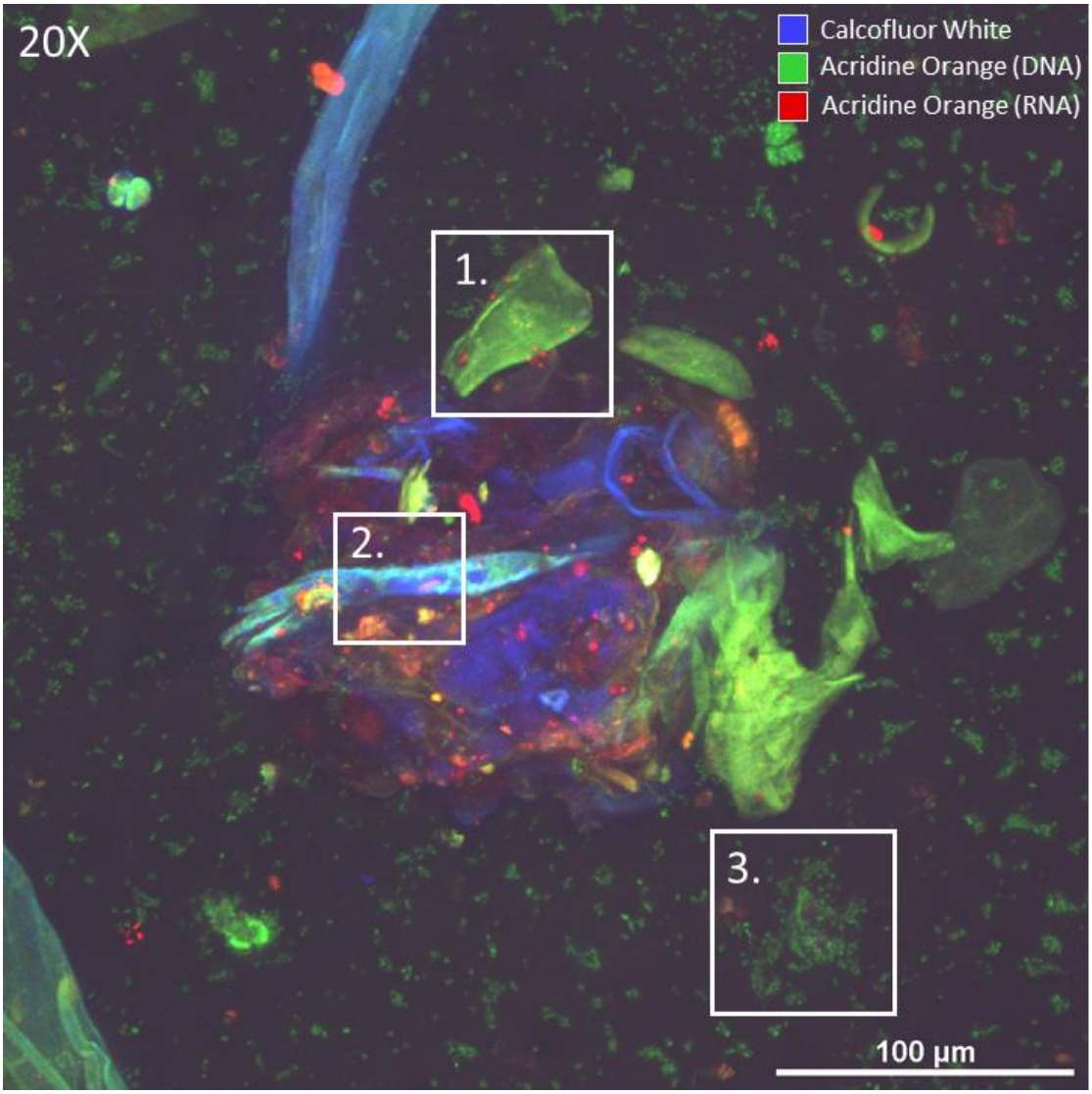

Fig. 4.1: Micrograph showing calcofluor white (fungi/algae; blue) and acridine orange (all DNA/RNA in green and red respectively) staining on house dust. 1 = human skin cell. 2 = fibres stained with both calcofluor white and acridine orange. 3 = microbes surrounding dust particle.

4.4 - Discussion

My results show some promise for future FISH-studies on dust particles. Fibres detected in this study are likely clothing fibres, explaining the variation in autofluorescence between fibres (i.e. different clothing dyes for different fibres) and their ability to absorb calcofluor white, as calcofluor white was originally used as a clothing brightener before its capacity to bind to fungal/algal cell walls was discovered (Hoch *et al*., 2005; Clark, 2011). The structure of dust matches that expected from previous studies (Morawska and Salthammer, 2006; Proietti *et al*., 2015). Strong autofluorescence was detected in 450 nm – 500 nm and 595 nm – 645 nm bands, but little in other bands examined. Dyes with sub >450 nm emission spectrums (i.e: DAPI, AlexaFluor405™) would be ideal for future studies. Autofluorescence could potentially be overcome using signal amplification techniques such as CARD-FISH.

This pilot study was limited by the time and resources available yet forms a good starting point. It is paramount to determine if tyramides used in CARD-FISH amplification also bind to clothing fibres. If not, CARD-FISH could be used to overcome issues encountered with autofluorescence. Autofluorescence reduction techniques are another option to be explored.

References

4',6-Diamidino-2-phenylindole. Available at: https://pubchem.ncbi.nlm.nih.gov/compound/2954 Accessed: 11/01/2022.

Ahmad, M., Liu, S., Mahmood, N., Mahmood, A., Ali, M., Zheng, M., Ni, J. (2017). Effects of Porous Carrier Size on Biofilm Development, Microbial Distribution and Nitrogen Removal in Microaerobic Bioreactors. *Bioresource Technology*. 234:360-69.

Alawi, M., Lipski, A., Sanders, T., Pfeiffer, E.V., Spieck, E. (2007). Cultivation of a Novel Cold-Adapted Nitrite Oxidizing Betaproteobacterium from the Siberian Arctic. *ISME J*. 1(3):256-64.

Ali, M., Oshiki, M., Rathnayeke, L., Ishii, S., Satoh, H., Okabe, S. (2016). Rapid and Successful Start-Up of Anammox Process by Immobilizing the Minimal Quantity of Biomass in PVA-SA Gel Beads. *Water Res*. 79:147-57.

Alves, R.E.V., Minh, B.Q., Urich T., von Haeseler, A., Schleper, C. (2018). Unifying the Global Phylogeny and Environmental Distribution of Ammonia-Oxidising Archaea Based on *amoA* Genes. *Nat Commun*. 9(1517).

Amann, R.I., Binder, B.J., Olson, R.J., Chisholm, S.W., Devereux, R., and Stahl, D.A. (1990). Combination of 16S rRNA-Targeted Oligonucleotide Probes with Flow Cytometry for Analyzing Mixed Microbial Populations. *Appl Environ Microbiol.* 56(6):1919-25.

Amend, A.S., Seifert, K.A., Samson, R., Bruns, T.D. (2010). Indoor fungal composition is geographically patterned and more diverse in temperate zones than in the tropics. *PNAS*. 107(31):13748-53.

Arunakirinathan, K., Heindl, A. (2022). Fishalyser: Fishalyser a Package for Automated Fish Quantification. R Package Version 1.32.0.

Bae, H., Choi, M., Lee, C., Chung, Y., Yoo, Y.J., Lee, S. (2015). Enrichment of Anammox Bacteria from Conventional Activated Sludge Entrapped in Poly(Vinyl Alcohol)/Sodium Alginate Gel. *Chem Eng J*. 281:531-40.

Bankhead, P. (2014). Analyzing Fluorescence Microscopy Images with ImageJ. Available at: https://confocal.uconn.edu/wp-content/uploads/sites/1081/2016/02/2014-05_Analyzing_fluorescence_microscopy_images.pdf. Accessed: 30/07/22.

Bartosch, S., Hartwig, C., Spieck, F., Bock, E. (2002). Immunological Detection of *Nitrospira*-Like Bacteria in Various Soils. *Microbial Ecology*. 43(1):26–33.

Beeftink, H.H., Staugaard, P. (1986). Structure and Dynamics of Anaerobic Bacterial Aggregates in a Gas-Lift Reactor. *Appl Environ Microbiol*. 52(5):1139-46.

Birzele, L.T., Depner, M., Ege, M.J., Engel, M., Kublik, S., Bernau, C., Loss, G.J., Genuneit, J., Horak, E., Schloter, M., Braun-Fahrländer, C., Danielewicz, H., Heederik, D., von Mutius, E., Legatzki, A. (2017). Environmental and mucosal microbiota and their role in childhood asthma. *Allergy*. 72(1):109-119.

Blackburne, R., Vadivelu, V.M., Yuan, Z., Keller, J. (2007). Kinetic Characterisation of an Enriched *Nitrospira* Culture with Comparison to *Nitrobacter*. *Water Res*. 41(14):3033-42.

Born, M., Wolf, E. (1980). *Principles of Optics.* 6th Ed*. Pergamon Press Ltd.* Heading Hill Hall, Oxford.

Braker, G., Conrad, R. (2011). Diversity, Structure, and Size of N_2O-Producing Microbial Communities in Soils - What Matters for Their Functioning? *Adv Appl Microbiol*. 75:33-70.

Braker, G., Zhou, J., Wu, L., Devol, A.H., Tiedje, J.M. (2000). Nitrite Reductase Genes (*nirk* and *nirs*) as Functional Markers to Investigate Diversity of Denitrifying Bacteria in Pacific Northwest Marine Sediment Communities. *Appl Environ Microbiol.* 66(5):2096-104.

Cabello, P., Roldán, M.D., Moreno-Vivián, C. (2004). Nitrate Reduction and the Nitrogen Cycle in Archaea. *Microbiology.* 150(11):3527-46.

Cao, Y., van Loosdrecht, M.C.M., Daigger, G.T. (2017). Mainstream Partial Nitritation-Anammox in Municipal Wastewater Treatment: Status, Bottlenecks, and Further Studies. *Appl Microbiol Biotechnol*. 101(4):1365-83.

Castro-Sowinski, S. (2019). The Ecological Role of Micro-Organisms in the Antarctic Environment. 1st Ed. Ch 10:221-37. *Springer International Publishing*. Cham, Switzerland.

Clark, D.R., McKew, B.A., Dong, L.F., Leung, G., Dumbrell, A.J., Stott, A., Grant, H., Nedwell, D.B., Trimmer, M., Whitby, C. (2020). Mineralization and Nitrification: Archaea Dominate Ammonia-Oxidising Communities in Grassland Soils. *Soil Biology and Biochemistry.* 143:107725.

Clark, M. (2011). Handbook of Textile and Industrial Dyeing: Principles, Processes and Types of Dyes. 1st Ed. *Woodhead Publishing Ltd*. Sawston, UK.

Cook, P.L.M., Kessler, A.J., Eyre, B.D. (2017). Does Denitrification Occur Within Porous Carbonate Sand Grains? *Biogeosciences*. 14(18):4061-69.

Correll, D.L. (1998). The Role of Phosphorus in the Eutrophication of Receiving Waters: A Review. *Journal of Environmental Quality*. 27(2):261-266.

Daims, H., Lebedeva, E.V., Pjevac, P., Han, P., Herbold, C., Albertsen, M., Jehmlich, N., Palatinszky, M., Vierheilig, J., Bulaev, A., Kirkegaard, R.H., von Bergen, M., Rattei, T., Bendinger, B., Nielsen, P.H., Wagner, M. (2015). Complete Nitrification by *Nitrospira* Bacteria. *Nature*. 528(7583):504-9.

Daims, H., Nielsen, J.L., Nielsen, P.H., Schleifer, K., Wagner, M. (2001). In Situ Characterization of *Nitrospira*-Like Nitrite-Oxidizing Bacteria Active in Wastewater Treatment Plants. *Appl Environ Microbiol*. 67(11):5273-84.

de los Ríos, A., Grube, M., Sancho, L.G., Ascaso, C. (2006). Ultrastructural and Genetic Characteristics of Endolithic Cyanobacterial Biofilms Colonizing Antarctic Granite Rocks. *FEMS Micro Ecol*. 59(2):386-395.

Dodds, W.K., Bouska, W.W., Eitzmann, J.L., Pilger, T.J., Pitts, K.L., Riley, A.J., Schloesser, J.T., Thornbrugh, D.J. (2009). Eutrophication of U.S. Freshwaters: Analysis of Potential Economic Damages. *Environ Sci Technol.* 43(1):12-9.

Fischer, K., Barbier, G.G., Hecht, H., Mendel, R.R, Campbell, W.H., Schwarz, G. (2005). Structural Basis of Eukaryotic Nitrate Reduction: Crystal Structures of the Nitrate Reductase Active Site. *Plant Cell*. 17(4):1167-79.

Fowler, S.J., Palomo, A., Dechesne, A., Mines, P.D., Smets, B.F. (2018). Comammox *Nitrospira* Are Abundant Ammonia Oxidizers in Diverse Groundwater-Fed Rapid Sand Filter Communities. *Environ Microbiol*. 20(3):1002-15.

French, E., Kozlowski, J.A., Mukherjee, M., Bullerjahn, G., Bollmann, A. (2012). Ecophysiological Characterization of Ammonia-Oxidizing Archaea and Bacteria from Freshwater. *Appl Environ Microbiol*. 78(16):5773-80.

Galloway, J.N., Aber, J.D., Erisman, J.W., Seitzinger, S.P., Howarth, R.W., Cowling, E.B., and Cosby, B.J. (2003). The Nitrogen Cascade. *BioScience.* 53(4):341-56.

Galloway, J.N., Dentener, F.J., Capone, D.G., Boyer, E.W., Howarth, R.W., Seitzinger, S.P., Asner, G.P., Cleveland, C.C., Green, P.A., Holland, E.A., Karl, D.M., Michaels, A.F., Porter, J.H., Townsend, A.R., Vöosmarty, C.J. (2004). Nitrogen Cycles: Past, Present, and Future. *Biogeochemistry*. 70:153-226.

Gottshall, E.Y., Bryson, S.J., Cogert, K.I., Landreau, M., Sedlacek, C.J., Stahl, D.A., Daims, H., Winkler, M. (2021). Sustained Nitrogen Loss in a Symbiotic Association of Comammox *Nitrospira* and AnAOB. *Water Res*. 202(117426).

Gould, G.W., Lees, H. (1960). The Isolation and Culture of the Nitrifying Organisms. *Canadian Journal of Microbiology*. 6(3):299-307.

Garcia-Pichel, F. (2006). Plausible Mechanisms for the Boring on Carbonates by Microbial Phototrophs. *Sedimentary Geology.* 185:205-13.

Hastings, R.C., Ceccherini, M.T., Miclaus, N., Saunders, J.R., Bazzicalupo, M., McCarthy, A.J. (1997). Direct Molecular Biological Analysis of Ammonia Oxidising Bacteria Populations in Cultivated Soil Plots Treated with Swine Manure. *FEMS Micro Ecol*. 23(1):45-54.

Head, I.M., Hiorns, W.D., Embley,T.M. McCarthy, A.J., Saunders, J.R. (1993). The Phylogeny of Autotrophic Ammonia-Oxidising Bacteria as Determined by Analysis of 16S Ribosomal RNA Gene Sequences. *Microbiology*. 139(6):1147-53.

Heppell, C.M., Binley, A., Trimmer, M., Darch, T., Jones, A., Malone, E., Collins, A.L., Johnes, P.J., Freer, J.E., Lloyd, C.E.M. (2017). Hydrological Controls on Doc: Nitrate Resource Stoichiometry in a Lowland, Agricultural Catchment, Southern UK. *Hydrol. Earth Syst. Sci.* 21(9):4785-802.

Hirsch, M.D., Long, Z.T., Song, B. (2011). AnAOB Diversity in Various Aquatic Ecosystems Based on the Detection of Hydrazine Oxidase Genes (*hzoa*/*hzob*). *Microb Ecol*. 61(2):264-76.

Hoch, H.C., Galvani, C.D., Szarowski, D.H., Turner, J.N. (2005). Two new fluorescent dyes applicable for visualization of fungal cell walls. *Mycologia*. 97(3):580-8.

Hovanec T.A., DeLong, E.F. (1996). Comparative Analysis of Nitrifying Bacteria Associated with Freshwater and Marine Aquaria. *Appl Environ Microbiol*. 62(8):2888-96.

Hu, Z., Lotti, T., van Loosdrecht, M., Kartal, B. (2013). Nitrogen Removal with the Anaerobic Ammonium Oxidation Process. *Biotechnol Lett*. 35(8):1145-54.

Humbert, S., Zopfi, J., and Tarnawski, S. (2012). Abundance of AnAOB in Different Wetland Soils. *Environmental Microbiology Reports*. 4(5):484-90.

Ishii, K., Mussmann, M., MacGregor, B.J., Amann, R. (2004). An Improved Fluorescence in Situ Hybridization Protocol for the Identification of Bacteria and Archaea in Marine Sediments. *FEMS Microbiol Ecol*. 50(3):203-13.

Jahnke, R. (1985). A Model of Microenvironments in Deep-Sea Sediments: Formation and Effects on Porewater Profiles. *Limnology and Oceanography*. 30(5):966-71.

Jung, M., Sedlacek, C.J., Kits, K.D., Mueller, A.J., Rhee, S., Hink, L., Nicol, G.W., Bayer, B., Lehtovirta-Morley, L., Wright, C., de la Torre, J.R., Herbold, C.W., Pjevac, P., Daims, H., Wagner, M. (2021). Ammonia-oxidising Archaea Possess a Wide Range of Cellular Ammonia Affinities. *ISME J*. 16(1):272-283.

Kalvelage, T., Jensen, M.M., Contreras, S., Revsbech, N.P., Lam, P., Günter, M., LaRoche, J., Lavik, G., Kuypers, M.M.M. (2011). Oxygen Sensitivity of Anammox and Coupled N-Cycle Processes in Oxygen Minimum Zones. *PLOS ONE*. 6(12):e29299.

Kamp, A., Høgslund, S., Risgaard-Petersen, N., Stief, P. (2015). Nitrate Storage and Dissimilatory Nitrate Reduction by Eukaryotic Microbes. *Front Microbiol*. 6(1492).

Kartal, B., Keltjens, J.T. (2016) Anammox Biochemistry: A Tale of Heme C Proteins. *Trends Biochem Sci*. 41(12):998-1011.

Kartal, B., Kuenen, J.G., van Loosdrecht, M.C.M. (2010). Engineering. Sewage Treatment with Anammox. *Science*. 328(5979):702-3.

Ke, X., Angel, R., Lu, Y., Conrad, R. (2013). Nitrifiers in Rice Paddy Soil. *Environ Microbiol*. 15:2275-92.

Keilluweit, M., Gee, K., Denney, A., Fendorf, S. (2018). Anoxic Microsites in Upland Soils Dominantly Controlled by Clay Content. *Soil Biology and Biochemistry*. 118:42-50.

Koch, H., van Kessel M.A.H.J., Lücker, S. (2019). Complete Nitrification: Insights into the Ecophysiology of Comammox *Nitrospira*. *Appl Microbiol Biotechnol*. 103(1):177–89.

Kubota, K. (2013). Card-Fish for Environmental Microorganisms: Technical Advancement and Future Applications. *Microbes Environ*. 28(1):3-12.

Perkins, R., Halsey, S.D. (1971). Geologic Significance of Microboring Fungi and Algae in Carolina Shelf Sediments. *J Sedimentary Res*. 41(3):843-53.

Kuypers, M.M.M., Marchant, H.K., Kartal, B. (2018). The Microbial Nitrogen-Cycling Network. *Nat Rev Microbiol*. 16(5):263-76.

Lansdown, K., McKew, B.A., Whitby, C., Heppell, C., Dumbrell, A.J., Binley, A., Olde, L., and Trimmer, M. (2016). Importance and Controls of Anaerobic Ammonium Oxidation Influenced by Riverbed Geology. *Nature Geoscience*. 9(5):357-60.

Lehnert, N., Dong, H.T., Harland, J.B., Hunt, A.P., and White, C.J. (2018). Reversing Nitrogen Fixation. *Nature Reviews Chemistry*. 2(10):278-89.

Lehtovirta-Morley, L.E. (2018). Ammonia Oxidation: Ecology, Physiology, Biochemistry and Why They Must All Come Together. *FEMS Microbiol Lett*. 365(9):fny058.

Ma, W., Li, G., Huang, B., Jin, R. (2020). Advances and Challenges of Mainstream Nitrogen Removal from Municipal Wastewater with Anammox-Based Processes. *Water Env Res*. 92(11):1899-1909.

McTavish, H., Fuchs, J.A., Hooper, A.B. (1993). Sequence of the Gene Coding for Ammonia Monooxygenase in *Nitrosomonas europaea*. *J Bacteriol*. 175(8):2436–2444.

Morawska, L., Salthammer, T. (2006). Indoor Environment: Airborne Particles and Settled Dust. 2nd Ed. *John Wiley and Sons*. Hoboken, NJ.

Nowak, O., Svardal, K., Kroiss, H. (1996). The Impact of Phosphorus Deficiency on Nitrification – Case Study of a Biological Pretreatment Plant for Rendering Plant Effluent. *Water Sci Technol*. 34(1-2):229-36.

Nowka, B., Daims, H., Spieck, E. (2015). Comparison of Oxidation Kinetics of Nitrite-Oxidizing Bacteria: Nitrite Availability as a Key Factor in Niche Differentiation. *Appl Environ Microbiol*. 81(2):745-53.

Pawley, J. (2000). The 39 Steps: A Cautionary Tale of Quantitative 3-D Fluorescence Microscopy. *Biotechniques*. 28(5):884-6.

Pernthaler, A., Pernthaler, J., Amann, R. (2002). Fluorescence in Situ Hybridization and Catalyzed Reporter Deposition for the Identification of Marine Bacteria. *Appl Environ Microbiol*. 68(6):3094-101.

Pester, M., Maixner, F., Berry, D., Rattei, T., Koch, H., Lücker, S., Nowka, B., Richter A., Spieck, E., Lebedeva, E., Loy, A., Wagner, M., Daims, H. (2014). *nxrB* Encoding the Beta Subunit of Nitrite Oxidoreductase as Functional and Phylogenetic Marker for Nitrite-oxidizing *Nitrospira*. *Environ Microbiol*. 16(10):3055-71.

Pjevac, P., Schauberger, C., Poghosyan, L., Herbold, C.W., van Kessel, M.A.H.J., Daebeler, A., Steinberger, M., Jetten, M.S.M., Lücker, S., Wagner, M., Daims, H. (2017). *amoA*-targeted Polymerase Chain Reaction Primers for the Specific Detection and Quantification of Comammox *Nitrospira* in the environment. *Front Microbiol*. 8(11):1508.

Pretty, J.N., Mason, C.F., Nedwell, D.B., Hine, R.E., Leaf, S., Dils, R. (2003). Environmental Costs of Freshwater Eutrophication in England and Wales. *Environ Sci Technol*. 37(2):201-8.

Probandt, D., Eickhorst, T., Ellrott, A., Amann, R., Knittel, K. (2018). Microbial Life on a Sand Grain: From Bulk Sediment to Single Grains. *ISME J*. 12(2):623-33.

Proietti, A., Panella, M., Leccese, F., Svezia, E. (2015). Dust Detection and Analysis in Museum Environment Based on Pattern Recognition. *Measurement*. 66:62-72.

Prosser, J.I., Nicol, G.W. (2012). Archaeal and Bacterial Ammonia-oxidisers in Soil: The Quest for Niche Specialisation and Differentiation. *Trends Microbiol*. 20(11):523-531.

Purchase, B.S. (1974). The Influence of Phosphate Deficiency on Nitrification. *Plant and Soil*. 41:541-47.

Raj, A., van den Bogaard, P., Rifkin, S.A., van Oudenaarden, A., Tyagi, S. (2008). Imaging Individual mRNA Molecules Using Multiple Singly Labelled Probes. *Nat Methods*. 5(10):877-9.

Ramírez-Reinat, E.L.., Garcia-Pichel, F. (2012). Prevalence of Ca^{2+}-Atpase Mediated Carbonate Dissolution among Cyanobacterial Euendoliths. *Appl Environ Microbiol*. 78(1):7-13.

Rao, A.M.F, McCarthy, M.J., Gardner, W.S., Jahnke, R.A. (2007). Respiration and Denitrification in Permeable Continental Shelf Deposits on the South Atlantic Bight: Rates of Carbon and Nitrogen Cycling from Sediment Colum Experiments. *Continental Shelf Res*. 27(13):1801-19.

Ratan, Z.A., Zaman, S.B., Mehta, V., Haidere, M.F., Runa, N.J., Akter, N. (2017). Application of Fluorescence in Situ Hybridization (FISH) Technique for the Detection of Genetic Aberration in Medical Science. *Cureus*. 9(6):e1325.

Rennke, H.G., Venkatachalam, M.A. (1979). Chemical Modification of Horseradish Peroxidase. Preparation and Characterization of Tracer Enzymes with Different Isoelectric Points. *J Histochem Cytochem*. 27(10):1352-53.

Rintala, H., Pitkäranta, M., Täubel, M. (2012). Microbial Communities Associated with House Dust. *Adv Appl Microbiol.* 78:75-120.

Rockström, J., Steffen, W., Noone, K., Persson, A., Stuart, F.C., Lambin, E.F., Lenton, T.M., Scheffer, M., Folke, C., Schnellnhuber, H.J., Nykvist, B., de Wit, C.A., Hughes, T., der Leeuw, S., Rodhe, H., Sorlin, S., Snyder, P.K., Costanza, R., Svedin, U., Falkenmark, M., Karlberg, L., Corell, R.W., Fabry, V.J.,

Hanses, J., Walker, B., Liverman, D., Richardson, K., Crutzen, P., Foley, J.A. (2009). A Safe Operating Space for Humanity. *Nature*. 461(7263):472-75.

Roush, D., Garcia-Pichel, F. (2020). Succession and Colonization Dynamics of Endolithic Phototrophs within Intertidal Carbonates. *Microorganisms*. 8(2):214.

Salles, J.F., Poly, F., Schmid, B., le Roux, X. (2009). Community Niche Predicts the Functioning of Denitrifying Bacterial Assemblages. *Ecology*. 90(12):3324-32.

Scarlett, K., Denman, S., Clark, D.R., Forster, J., Vangeulova, E., Brown, N., Whitby, C. (2021). Relationships between Nitrogen Cycling Microbial Community Abundance and Composition Reveal the Indirect Effect of Soil pH on Oak Decline. *ISME J*. 15(3):623–635.

Schaubroeck, T., De Clippeleir, H., Weissenbacher, N., Dewulf, J., Boeckx, P., Vlaeminck, S., Wett, B. (2015). Environmental Sustainability of an Energy Self-Sufficient Sewage Treatment Plant: Improvements through Demon and Co-Digestion. *Water Res*. 74:166-79.

Schindelin, J., Arganda-Carreras, I., Frise, E., Kaynig, V., Longair, M., Pietzsch, T., Preibisch, S., Rueden, C., Saalfeld, S., Schmid, B., Tinevez, J, White, D.J., Hartenstein, V., Eliceiri, K., Tomancak, P., Cardona, A. (2012). Fiji: An Open-Source Platform for Biological-Image Analysis. *Nat Methods*. 9(7): 676-82.

Schmid, M., Thill, A., Purkhold, U., Walcher, M., Bottero, J., Ginestet, P., Nielsn, H., Wuertz, S., Wagner, M. (2003). Characterization of Activated Sludge Flocs by Confocal Laser Scanning Microscopy and Image Analysis. *Water Res*. 37(9):2043-52.

Schmid, M. (2008). Accurate Gaussian Blur. Available at: https://imagej.nih.gov/ij/plugins/gaussian-blur.html. Accessed: 11/11/22.

Siegrist, H., Salzgeber, D., Eugster, J., Joss, A. (2008). Anammox Brings WWTP Closer to Energy Autarky Due to Increased Biogas Production and Reduced Aeration Energy for N-Removal. *Water Sci Technol*. 57(3):383-8.

Simon, J., Klotz, M.G. (2013). Diversity and Evolution of Bioenergetic Systems Involved in Microbial Nitrogen Compound Transformations. *Biochim Biophys Acta*. 1827(2):114-35.

Sonthiphand, P., Hall, M.W., Neufeld, J.D. (2014). Biogeography of Anaerobic Ammonia-Oxidizing (Anammox) Bacteria. *Front Microbiol*. 5:399.

Sorokin, D.Y., Lücker, S., Vejmelkova, D., Kostrikina, N.A., Kleerebezem, R., Rijpstra, W.I.C., Damste, J.S.S., Le Paslier, D., Muyzer, G., Wagner, M., van Loosedrecht, M.C.M., Daims, H. (2012). Nitrification Expanded: Discovery, Physiology and Genomics of a Nitrite-Oxidizing Bacterium from the Phylum Chloroflexi. *ISME J*. 6(12):2245–2256.

Spears, B.M., Andrews, C., Banin, L., Carvalho, L., Cole, S., De Ville, M., Gunn, I.D.M., Ives, S., Lawlor A., Leaf, S., Lofts, S., Maberly, S.C., Madgwick, G., May, L., Moore, A., Pitt, J., Smith, R., Waters, K., Watt, J., Winfield, I.J., Woods, H. (2018). Assessment of Sediment Phosphorus Capping to Control Nutrient Concentrations in English Lakes. 1st Ed. *UK Environment Agency*. Bristol, UK.

Speicher, M.R., Carter, N.P. (2005). The New Cytogenetics: Blurring the Boundaries with Molecular Biology. *Nat Rev Genet*. 6(10):782-92.

Straka, L.L., Meinhardt, K.A., Bollmann, A., Stahl, D.A., Winkler, M.H. (2019). Affinity Informs Environmental Cooperation between Ammonia-Oxidizing Archaea (AOA) and Anaerobic Ammonia-Oxidizing (Anammox) Bacteria. *ISME J*. 13(8):1997-2004.

Swedlow, J.R. (2013). Quantitative Fluorescence Microscopy and Image Deconvolution. *Methods Cell Biol*. 114:407-26.

Thompson, J.R., Argyraki, A., Bashton, M., Bramwell, L., Crown, M., Hursthouse, A.S., Jabeen, K., Reis, P.M., Namdeo, A., Nelson A., Pearce, D.A., Potgieter-Vermaak, S., Rasmussen, P.E., Wragg, J., Entwistle, J.A. (2021). Bacterial Diversity in House Dust: Characterization of a Core Indoor Microbiome. *Front. Envon. Sci.* 9(754657).

Treusch, A.H., Leininger, S., Kletzin, A., Schuster, S.C., Klenk, H., Schleper, C. (2005). Novel Genes for Nitrite Reductase and Amo-related Proteins Indicate a Role of Uncultivated Mesophilic Crenarchaeota in Nitrogen Cycling. *Environ Microbiol*. 7(12):1985-95.

van de Graaf, A.A., Mulder, A., de Bruijn, P., Jetten, M.S., Robertson, L.A., and Kuenen, J.G. (1995). Anaerobic Oxidation of Ammonium Is a Biologically Mediated Process. *Appl Environ Microbiol*. 61(4):1246-51.

van Gijlswijk, R.P., Wiegant, J., Raap, A.K., and Tanke, H.J. (1996). Improved Localization of Fluorescent Tyramides for Fluorescence in Situ Hybridization Using Dextran Sulfate and Polyvinyl Alcohol. *J Histochem Cytochem*. 44(4):389-92.

van Niftrik, L.A., Fuerst, J.A., Damsté, J.S.S, Kuenen, J.G., Jetten, M.S.M., Strous, M. (2004). The Anammoxosome: An Intracytoplasmic Compartment in Anammox Bacteria. *FEMS Microbiology Letters*. 233(1):7–13.

Vlaeminck, S.E., Cloetens, L.F.F., Carballa, M., Boon, N., Verstraete, W. (2008). Granular Biomass Capable of Partial Nitritation and Anammox. *Water J Sci Technol*. 58(5):1113-20.

Wada, N., Pollock, F.J., Willis, B.L., Ainsworth, T., Mano, N., and Bourne, D.G. (2016). In Situ Visualization of Bacterial Populations in Coral Tissues: Pitfalls and Solutions. *Peer J*. 4:e2424.

Wallner, G., Amann, R., Beisker, W. (1993). Optimizing Fluorescent in Situ Hybridization With rRNA-Targeted Oligonucleotide Probes for Flow Cytometric Identification of Microorganisms. *Cytometry.* 14(2):136-43.

Ward, B.B., O'Mullan, G.D. (2002). The Distribution of *Nitrosococcus oceani*, a Marine Ammonia-Oxizdizing Gamma-Proteobacterium, Detected by PCR and Sequencing of 16S rRNA and *amoA* Genes. *Appl Environ Microbiol*. 68(8):4153–57.

Watson, S.W., Waterbury, J.B. (1971). Characteristics of Two Marine Nitrite Oxidizing Bacteria, *Nitrospina gracilis* nov. gen. nov. sp. and *Nitrococcus mobilis* nov. gen. nov. sp. *Archiv. Mikrobiol*. 77(3):203–30.

Wertz, S., Degrange, V., Prosser, J.I., Poly, F., Commeaux, C., Freitag, T., Guillaumand, N., le Roux, X. (2006). Maintenance of Soil Functioning Following Erosion of Microbial Diversity. *Environ Microbiol*. 8(12):2162-9.

Wertz, S., Degrange, V., Prosser, J.I., Poly, F., Commeaux, C., Guillaumand, N., le Roux, X. (2007). Decline of Soil Microbial Diversity does not Influence the Resistance and Resilience of Key Soil Microbial Functional Groups Following a Model Disturbance. *Environ Microbiol*. 9(9):2211-9.

Wett, B. (2007). Development and Implementation of a Robust Deammonification Process. *Water Sci Technol*. 56(7):81-88.

Wierzchos, J., Cámara, B., de Los Ríos, A., Davila, A.F., Sánchez Almazo, I.M., Artieda, O., Wierzchos, K., Gómez-Silva, B., McKay, C., Ascaso, C. (2011). Microbial Colonization of Ca-Sulfate Crusts in the Hyperarid Core of the Atacama Desert: Implications for the Search for Life on Mars. *Geobiology*. 9(1):44-60.

Woebken, D., Fuchs, B.M., Kuypers, M.M.M., Amann, R. (2007). Potential Interactions of Particle-Associated AnAOB with Bacterial and Archaeal Partners in the Namibian Upwelling System. *Appl Environ Microbiol*. 73(14):4648-57.

Wu, L., Shen, M., Li, J., Huang, S., Li, Z., Yan, Z., Peng, Y. (2019). Cooperation between Partial-Nitrification, Complete Ammonia Oxidation (Comammox), and Anaerobic Ammonia Oxidation (Anammox) in Sludge Digestion Liquid for Nitrogen Removal. *Environ Pollut*. 254(Pt A):112965.

Yang, S., Peng, Y., Zhang, S., Han, X., Li, J., Zhang, L. (2021). Carrier Type Induces Anammox Biofilm Structure and the Nitrogen Removal Pathway: Demonstration in a Full-Scale Partial Nitrification/Anammox Process. *Bioresource Technology.* 334:125249.

Zucker, R.M., Price, O. (2001). Evaluation of Confocal Microscopy System Performance. *Cytometry.* 44(4):273-94.

Zhang, M., Daraz, U., Sun, Q., Chen, P., Wei, X. (2021). Denitrifier Abundance and Community Composition Linked to Denitrification Potential in River Sediments. *Environ Sci Pollut Res Int*. 28(37):51928-39.